journal of the international meteor organization

WGN

48:5
october 2020

Cygnid-Draconid Complex explored:
call for Kappa Cygnid observations in 2021

IMC 2020 special issue:

ISSN 1016-3115

WGN Vol. 48, No. 5, October 2020, pp. 129 – 162

Administrative

Meteor Science

Conferences

Front cover photo

IMO Event#2967-2020, fireball caught over Kansas on Friday, 2020 June 19. Photo courtesy: Max Olson.

Back over photo

Brilliant fireball close to the comet C/2020 F3 (NEOWISE), on the morning of 2020 July 19 at 00:36 CEST from Villard-sur-Doron, Auvergne-Rhône-Alpes, France. This fireball was seen over France, Belgium, and Germany and can be investigated at: `https://fireball.imo.net/members/imo_view/event/2020/3502`.
Photo courtesy: Philippe Jacquot, `http://www.philippejacquotphotography.fr`

Writing for WGN

This Journal welcomes papers submitted for publication. All papers are reviewed for scientific content, and edited for English and style. Instructions for authors can be found in WGN **45:1**, 1–5, and at `http://www.imo.net/docs/writingforwgn.pdf` .

Copyright

Legal address

International Meteor Organization, Jozef Mattheessensstraat 60, 2540 Hove, Belgium.

From the Treasurer — IMO Membership/WGN Subscription Renewal for 2021

Marc Gyssens

Renewal rates

Most members/subscribers whose membership/subscription has expired should have received a reminder email by the time you receive this issue of WGN. Via this way, we invite them again to renew for 2021.

The fees are as tabulated below. We are happy that we can offer WGN at the same cost as last year. We also continue to offer an electronic-only subscription at a reduced rate.

IMO Membership/WGN Subscription 2021				
Electronic + paper with surface mail delivery:		€26		US$ 32
Electronic + paper with airmail delivery (outside Europe only):		€49		US$ 60
Electronic only:		€21		US$ 25
Supporting membership:	add	€26	add	US$ 32

It is also possible to renew for two or more years in a row.

When you renew, give a few minutes of thought to becoming a **supporting member** by paying at least 26 EUR/32 USD extra. Smaller gifts are of course also appreciated. As you may know, there is an IMO Support Fund. With this Support Fund, we offer support to meteor-related projects. Our ability to provide this service to the meteor community depends primarily on the gifts we receive from supporting members!

Another way to help meteor workers with limited funds is to offer them a gift subscription.

We already thank all our members that will renew for their continued trust in our Organization!

Payment instructions

You first must log in into your account at the IMO website if you want to renew. For this purpose, click the log-in button in the upper right-hand corner. As login, use the email address on which you received my reminder email. In case you forgot your password, you can use the "forgot password" link to reset it. Once logged in, you will see your profile picture (or the space provided for it). If you read on the green button below it that your membership is about to expire, click it, and the rest will be self-explanatory.[1]

The outcome of this process is that you will see the total amount due and your payment options. If you choose to pay using PayPal (or using a credit card via PayPal), you can complete the payment on our website.

If you experience any difficulties, do not hesitate to contact me at `treasurer@imo.net`.

One final request: every year, a lot of members renew late. As a consequence, back issues that already appeared have to be sent out to these members. Please support our volunteers in their bimonthly effort to have WGN shipped to you by renewing promptly! Thank you for your understanding and cooperation!

IMO bibcode WGN-485-gyssens-renewals NASA-ADS bibcode 2020JIMO...48..129G

[1] Alternatively, you can also click on "Extend your membership" in the pull-down menu to the right of your name in the upper right-hand corner, with the same result.

Meteor Science

Cygnid-Draconid Complex (κ-Cygnids) II: Call for observations, κ-Cygnids 2021

Masahiro Koseki[1]

The κ-Cygnids have a periodic nature of 7 years (Koseki, 2014) and will show enhanced activity in 2021. The author has reanalyzed the details of the Cygnid-Draconid Complex (CDC) as determined by recent observations and would like to provide useful information for the next observing opportunity.
The CDC consists of four meteor activities. The early Cygnid activity before solar longitude $\lambda_s < 130°$ is not κ-Cygnids (shower #12 KCG in the IAU Meteor Data Center list) but July γ-Draconids (#184 GDR). AXD (August ξ-Draconids, formerly named as KCG3 in Koseki, 2014) is a weak activity but shows rather higher meteor rates than KCG in average years, and, moreover, it lies only about 5° west of KCG. ZDR (not ZDR in IAUMDC, see the text) becomes active before $\lambda_s < 150°$ when KCG and AXD are still active in the neighborhood. Observers are asked to examine the tables in the text to get useful and reliable results at the next opportunity. KCG observations are especially recommended during 2021 August 13 to 18, or λ_s range 140–145 degrees.

Received 2020 October 8

1 Introduction

We know KCG has a clear periodicity of 7 years (Koseki, 2014) and it would return again in 2021. We should prepare the observations of KCG 2021 with great care. It is said in the Chinese proverb, 'Know your enemies, know thyself, and you shall not fear a hundred battles.' We are going to study the nature of CDC using photographic observations and 3 video data sets at first. The 3 video data sets are EDMOND (Kornoš et al., 2014a,b), SonotaCo (SonotaCo, 2009) and CAMS (Jenniskens et al., 2016). The sources of the photographic data are described in Koseki (2009).

2 Analyses

The radiant drift can be represented as a short line in the orthographic projection for the Sun centered ecliptic coordinates $(\lambda - \lambda_s, \beta)$, for example GDR of Figures 1a–d, and we can get more accurate expressions by linear regression in such coordinates rather than as $\Delta\alpha$ and $\Delta\delta$. The radiant distributions around solar longitude $\lambda_s = 140°$ ($120 < \lambda_s < 160$) with the estimated drift (see Tables 2, 4, 6 and 8 for details) for three video data sets are shown in Figures 1a–c, while Figure 1d gives the results from photographic observations; photographic observations do not have enough data to estimate an exact radiant drift and the estimated lines in Figure 1d are of EDMOND. We can find four activities in this area and in this time range clearly; GDR, KCG, AXD (provisional name, see Section 3.3 AXD) and ZDR (formerly named AUD incorrectly in IAUMDC; see section 3.8.4 of Koseki, 2014). It is necessary to study these four showers together when we want to learn about KCG in depth.

2.1 Rotation

Figure 12 of Koseki (2014) suggests the KCG radiant area is strongly elongated and its axis is inclined to the longitude line of $\lambda - \lambda_s$ passing through the radiant center. It is better to modify the ordinary method we have used, for example in Koseki (2019), to extend the search area and to incline the axis. Figure 2a shows the ordinary radiant map centered at the preliminary radiant point given by the former study (Koseki, 2014); $(\lambda - \lambda_s, \beta) = (163.5, 70.2)$ during $\lambda_s = 139.5$–140.5. It is clear the radiant area is elongated and inclined and, therefore, we make the axis slant −20° (counterclockwise rotation) and set the search area as a rectangle shown in Figure 2b.

2.2 Iterations

We calculate the linear regressions of x and y on λ_s, where (x, y) are the coordinates of the radiant distribution centered at the shower radiant such as displayed in Figure 2b; it is natural to place the initial radiant point $(\lambda - \lambda_s, \beta)$ given in Table 1 at the center $(x, y) = (0, 0)$. The regression calculations were repeated as usual to become stable, as described in Koseki (2019); it was

Table 1 – Initial search areas. Δr is the radius in degrees of the limiting circle as shown in Figure 2a. Δx and Δy are the half lengths of the limiting rectangle as shown in Figure 2b for x-axis and y-axis. $\Delta\lambda_s$ is the half width of the duration (in solar longitude). θ is the rotation angle and minus means the rotation is counterclockwise.

Code	λ_s	$\lambda - \lambda_s$	β	Δr	Δx	Δy	$\Delta\lambda_s$	θ
GDR	124.6	167.9	73.0	3			5	0
KCG	142	168	74		3	6	12	−20
AXD	140	146.6	77.2		3	6	5	0
ZDR	155	47.5	81.6		3	6	5	−15

[1]The Nippon Meteor Society (NMS), 4-3-5 Annaka, Annaka-shi, Gunma-ken, 379-0116 Japan. Email: geh04301@nifty.ne.jp

IMO bibcode WGN-485-koseki-kcg
NASA-ADS bibcode 2020JIMO...48..130K

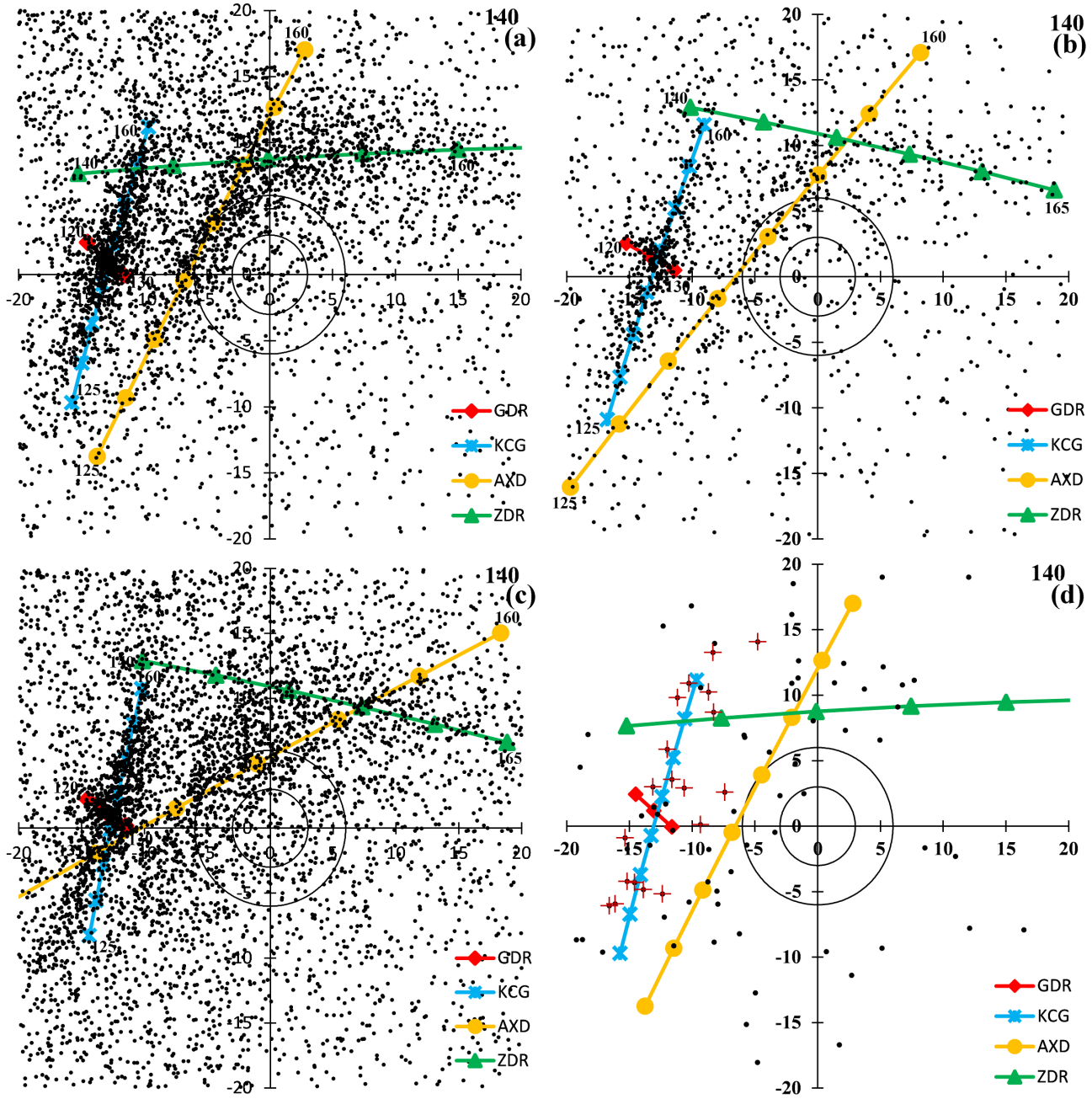

Figure 1 – Radiant distributions during $\lambda_s = 120$–160 centered at $(\lambda - \lambda_s, \beta) = (116, 78)$; y-axis runs through $\lambda - \lambda_s = 116$ and units are degrees. a: EDMOND, b: SonotaCo, c: CAMS, d: photographic (19 crosses are the 12+7 meteors mentioned in Section 3.2). The estimated radiant drifts are extended on both sides and do not represent their activity period; see the text for details.

necessary to repeat the iteration more than ten times except in the case of GDR, because the other three showers are very complex.

3 Results

Figures 1a–d give the summary results and clearly show the complexity of these activities; GDR crosses the KCG radiant path, AXD runs parallel with KCG and early ZDR activity overlaps with late AXD activity; we will study these problems in the following subsections. The iteration process works well except for CAMS' AXD, which seems to be in confusion with early KCG and ZDR (Figure 1c) We use mainly the EDMOND data for the radiant drift and the activity profiles, because SonotaCo net did not catch the 2014 KCG outburst fully, though we refer also to other observational data where appropriate.

3.1 GDR

GDR is quite distinct from KCG but its radiant drift crosses KCG's (Figures 1a–d). We should not classify radiating meteors near the estimated KCG radiant before $\lambda_s < 130$ as KCG; the geocentric velocity of GDR is nearly 10 km/s higher than that of early KCG (compare Tables 2 and 4). We give the radiant drift compensated distribution in Figure 3a and the activity profile in Figure 3b by the results of the radiant drift estimation of EDMOND data (Table 2). GDR has a clear radiant concentration in contrast to KCG and a sharp peak, and reaches the maximum at $\lambda_s = 125.2$: its activity

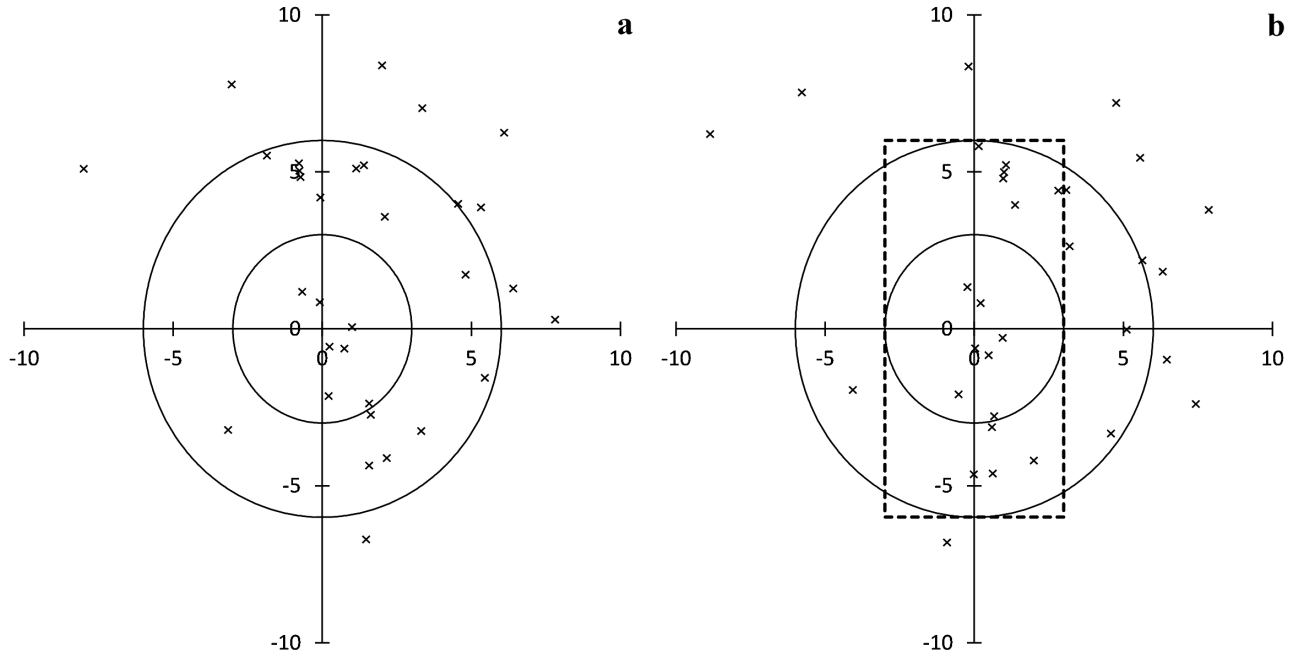

Figure 2 – An example drawing for the shower radiants during λ_s = 139.5–140.5 using SonotaCo net data centered at $(\lambda - \lambda_s, \beta) = (163.5\ 70.2)$. a: y-axis runs through $\lambda - \lambda_s = 163.5$, b: y-axis is rotated counterclockwise 20°.

period is short during λ_s = 124–127. We can catch its maximum exactly only if it occurs at nighttime wherever we live and, moreover, the weather should be fine. Table 3 shows GDR does not have a periodic nature like KCG. The GDR activity does seem to fluctuate year by year (Table 3) but the irregular peaks can be caused by such apparent observational condition changes. The peaks of the three data sets do not coincide with each other; total data numbers of EDMOND and CAMS are growing rapidly with year but SonotaCo net data is almost stable.

3.2 KCG

We give the radiant distribution, compensated by the radiant drift estimation, in Figure 4a and the activity profile in Figure 4b, computed from EDMOND data. It is necessary to note these figures are based mainly on 2014 observations, though EDMOND recorded only a small number of KCG in 2007 because EDMOND was at the dawning of its operation at that time (Table 5).

Both the radiant distribution and the estimated radiant drift coincide with the results of SonotaCo net and CAMS. It is suggested the radiant of KCG has not shifted between 2007 and 2014. Table 4 shows the estimated radiant point and geocentric velocity by the results of the iterations for EDMOND.

Figure 5 gives recorded KCG meteors within 3° from the estimated radiant ($Nr \leq 3$) as the moving mean within each 1° in λ_s. We cannot find a general maximum within these three observation sets; EDMOND reaches the maximum at λ_s = 144, CAMS at λ_s = 141 and SonotaCo net yields curious twin peaks at λ_s = 141 and λ_s = 145. It is necessary to note they are biased by observational conditions; EDMOND are mainly in 2014, CAMS does not include both 2007 and 2014 but recorded vast KCG numbers in 2010, SonotaCo net caught both events but 2014 observations were unfortunately interupted by bad weather during the maximum period.

Koseki (2014) suggested KCG might have bimodal peaks at λ_s=140 and λ_s=144. Whether the maximum of KCG might move or have bimodal peaks remains unsolved and 2021 observations could answer this question.

KCG were noticed in 1950 (Whipple, 1954) and followed by former Soviet observations in 1957 and 1964; Koseki (2014) selected 12 photographic KCG meteors by a D_{SH} search and now 7 photographic meteors are added by a radiant based search using EDMOND's radiant drift. Figure 6 represents the relation of the recorded λ_s with the year. It is also suggested the maximum of KCG might change year by year or have two peaks; the maximum may become earlier and this forward movement is valuable enough to check in future observations.

We should be careful to distinguish KCG from nearby activities: GDR, AXD and ZDR. KCG are active between λ_s = 130–155, though Figures 1a–d and Table 4 show the period extended on both sides for reference. It is also important to be aware of the increase of KCG velocity with time; the velocity becomes about 5 km/s faster in later activity than earlier (Table 4).

3.3 AXD

The author called this activity KCG3 (Koseki, 2014) but it is confirmed in this study as an independent activity (Figures 1a–d). We would like to name it August ξ-Draconids (AXD) temporarily. The greatest part of meteors classified as AXD in this study are identified as KCG both in EDMOND and SonotaCo net, though one third of classified 'AXD' meteors are labeled in CAMS as 'AUD' (that is, ZDR in this paper) and the other two thirds as KCG. It is not good to use the original classifications in those data sets to clarify the details of AXD activity.

Table 2 – The radiant estimation for GDR estimated from EDMOND iteration results.

λ_s	120	121	122	123	124	125	125.2	125.4	125.6	125.8	126	127	128	129	130
$\lambda - \lambda_s$	173.4	172.2	170.9	169.7	168.4	167.1	166.8	166.6	166.3	166.1	165.8	164.5	163.2	161.9	160.6
β	72.7	72.8	72.9	73.0	73.1	73.1	73.1	73.1	73.2	73.2	73.2	73.2	73.3	73.3	73.3
α	280.6	280.5	280.3	280.2	280.0	279.9	279.8	279.8	279.8	279.8	279.7	279.6	279.4	279.3	279.1
δ	50.1	50.2	50.3	50.3	50.4	50.4	50.4	50.4	50.5	50.5	50.5	50.5	50.5	50.5	50.5
V_g	27.7	27.5	27.4	27.2	27.0	26.8	26.8	26.7	26.7	26.6	26.6	26.4	26.2	26.1	25.9

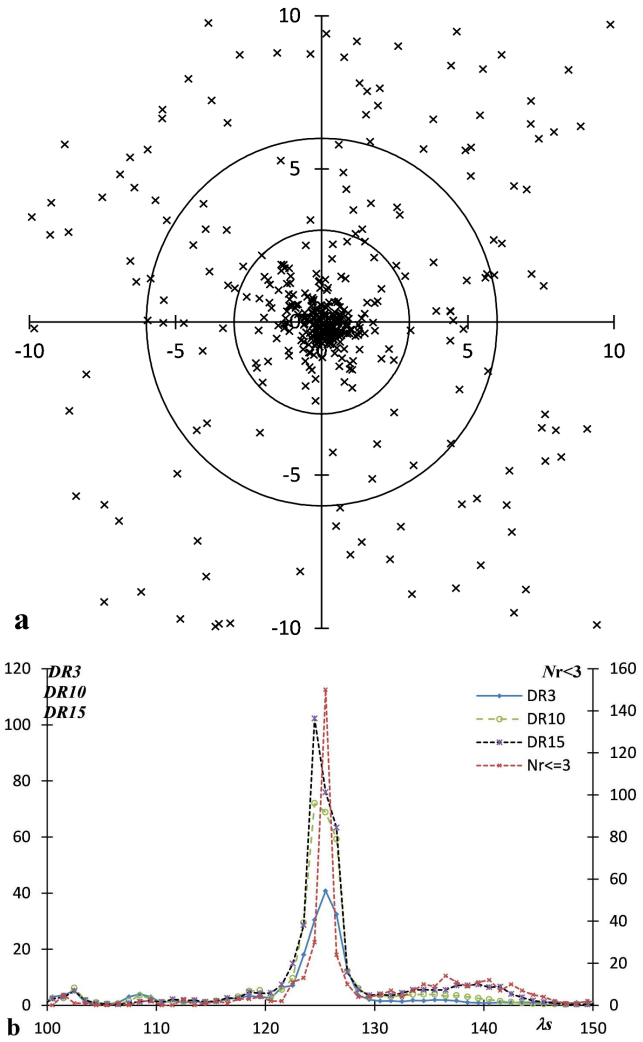

Figure 3 – Results of the iteration for GDR using EDMOND data. a: compensated radiant distribution; y-axis runs through $\lambda - \lambda_s = 167.9$ and units are degrees. b: activity profiles based on data compensated for radiant drift; $Nr \leq 3$ is the number of meteors within 3° from the estimated radiant point $(\lambda - \lambda_s, \beta)$ (see Table 2). DR3, DR10 and DR15 are the sliding mean of the radiant density ratios within bins of 3° in λ_s. DR3 is the density ratio within a circle of 3° relative to a ring of 3–6°. DR10 is the density ratio within a circle of 3° relative to a ring of 6–10°. DR15 is the density ratio within a circle of 3° relative to a ring of 10–15°.

We limit the period for study as $\lambda_s = 135$–145 because the discrimination between AXD and ZDR becomes difficult during $\lambda_s = 145$–150; radiant paths given in Figures 1a–d show early ZDR overlaps with late AXD activity around $\lambda_s = 150$.

Figure 7a shows AXD is clearly distinct from KCG but other activities including ZDR and sporadics prevent us from having a clear view of the AXD radiant distribution.

Table 3 – The yearly numbers of meteors classified as GDR. Unfortunately some early EDMOND data do not have correct observational dates; the numbers of EDMOND in 2004 include such erroneous dates and they should be associated with the following years.

Year	EDMOND	SonotaCo	CAMS
2004	15		
2005	1		
2006	0		0
2007	0	11	25
2008	7	11	32
2009	2	5	22
2010	3	8	38
2011	8	0	56
2012	17	2	33
2013	35	0	
2014	17	18	
2015	28	6	
2016	117	5	
2017		1	
2018		7	
Total	250	74	206

The activity profiles represented in Figure 7b are counted meteors and are calculated by using the extension of the estimated radiant drift (Table 6) for later than $\lambda_s = 145$. It is suggested the real maximum of AXD might be a little earlier than $\lambda_s = 145$ indicated in Figure 7b, because the counted meteors as shown Figure 7b could be contaminated by ZDR after $\lambda_s > 145$ and the real AXD meteor numbers might then become smaller than the values in the figure.

The estimated radiant drift for AXD could not be influenced by ZDR activity and, therefore, the extended path can suggest the probable AXD radiant point.

Though AXD is near to KCG with regard both to dates and to radiant position, Table 7 suggests AXD seems to be out of harmony with KCG. AXD activity did not soar in 2013 and 2014; AXD might be classified as 'KCG' in ordinary years because it seems to be more active than KCG in such years.

3.4 ZDR

The name 'AUD' is used incorrectly and this activity had been called ζ-Draconids (Koseki, 2014). One of the reasons for the confusion is because of the nearby AXD activity as described in Section 3.3.

We limit the period for study as $\lambda_s = 150$–160 because of the need to discriminate between AXD and

Table 4 – The radiant estimation for KCG estimated from EDMOND iteration results.

λ_s	125	130	131	132	133	134	135	136	137	138	139	140	141	142	143
$\lambda - \lambda_s$	152.9	155.5	156.1	156.7	157.3	158.0	158.7	159.5	160.3	161.1	162.0	163.0	163.9	165.0	166.1
β	63.3	66.1	66.7	67.3	67.8	68.4	68.9	69.5	70.0	70.6	71.1	71.7	72.2	72.7	73.3
α	274.6	278.5	279.3	280.0	280.7	281.4	282.1	282.8	283.5	284.2	284.8	285.4	286.0	286.6	287.2
δ	39.9	43.1	43.8	44.5	45.1	45.8	46.5	47.2	47.9	48.6	49.3	50.0	50.7	51.4	52.2
V_g	18.9	20.0	20.2	20.4	20.6	20.8	21.0	21.2	21.4	21.6	21.9	22.1	22.3	22.5	22.7
λ_s	144	145	146	147	148	149	150	151	152	153	154	155	160		
$\lambda - \lambda_s$	167.3	168.5	169.9	171.3	172.8	174.4	176.2	178.0	180.0	182.2	184.4	186.9	201.7		
β	73.8	74.3	74.8	75.3	75.8	76.3	76.7	77.2	77.6	78.0	78.4	78.8	80.4		
α	287.8	288.3	288.8	289.4	289.8	290.3	290.7	291.1	291.5	291.9	292.2	292.5	293.3		
δ	52.9	53.6	54.4	55.1	55.9	56.6	57.4	58.1	58.9	59.6	60.4	61.2	65.0		
V_g	22.9	23.1	23.3	23.5	23.7	23.9	24.2	24.4	24.6	24.8	25.0	25.2	26.3		

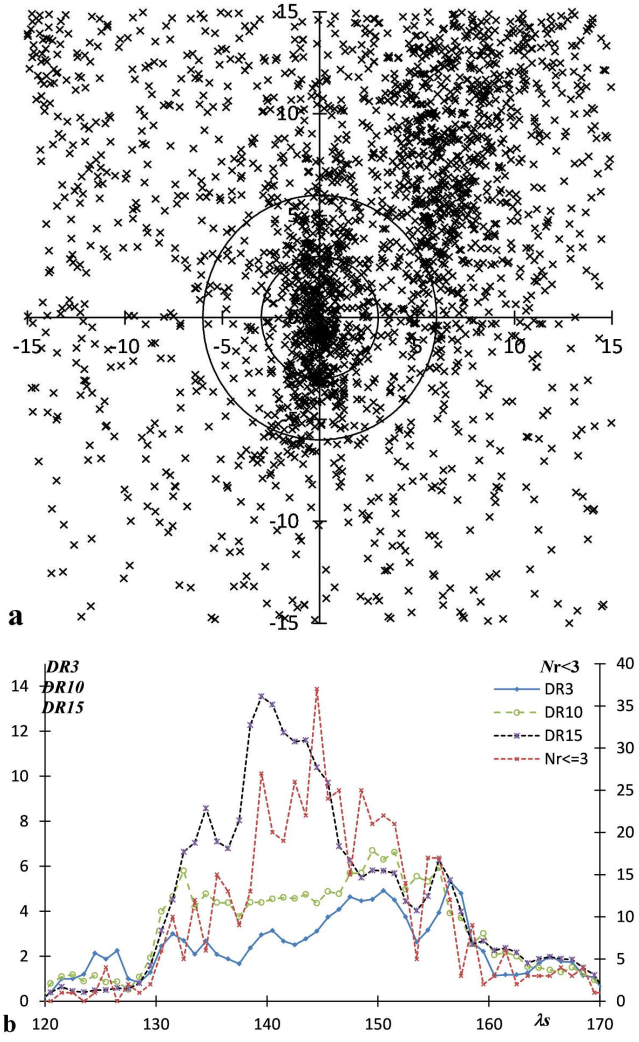

Figure 4 – Results of the iteration for KCG using EDMOND data. a: compensated radiant distribution; y-axis runs through $\lambda - \lambda_s = 168.0$. b: activity profiles based on data compensated for radiant drift. Detailed explanations are same as Figure 3.

Table 5 – The yearly numbers of meteors classified as KCG. EDMOND data in 2004 is incorrect (see Table 3).

Year	EDMOND	SonotaCo	CAMS
2004	8		
2005	0		
2006	0		0
2007	8	135	16
2008	1	2	15
2009	3	5	75
2010	5	8	538
2011	9	2	24
2012	13	7	25
2013	47	20	
2014	571	93	
2015	14	4	
2016	16	5	
2017		0	
2018		2	
Total	695	283	693

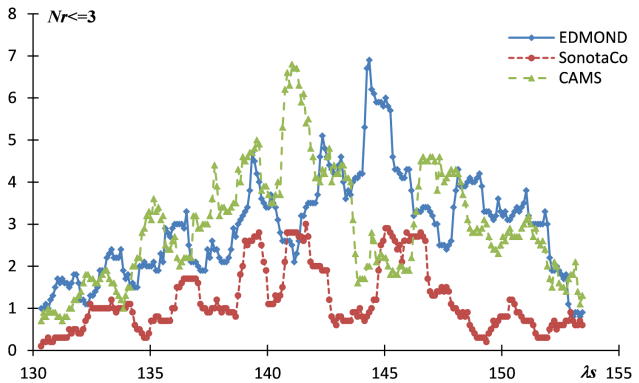

Figure 5 – Difference in three data sets of video observations, in meteor numbers within 3° from estimated KCG radiant point, plotted as the moving mean within 1° bins in λ_s; radiant drifts used here are estimated from respective observational data sets, not EDMOND only.

ZDR. The compensated radiant distribution (Figure 8a) shows the separation of ZDR from AXD is good enough and the radiant drift estimation (Table 8) might be enough to be practical for observations. The activity profiles before $\lambda_s < 150$ are the extended ones and, therefore, the peak of $Nr \leq 3$ might be caused by the mixture of two activities, AXD and ZDR (Figure 8b). The maximum of ZDR activity might be around $\lambda_s = 155$; this presumption is confirmed in the two data sets, SonotaCo net and CAMS. ZDR activity is out of harmony with KCG activity and is clearly an independent activity (Table 9).

Table 6 – The radiant estimation for AXD estimated from EDMOND iteration results.

λ_s	125	130	131	132	133	134	135	136	137	138	139	140	141	142	143
$\lambda - \lambda_s$	144.9	144.9	144.9	144.9	145.0	145.0	145.0	145.0	145.0	145.0	145.0	145.0	145.0	145.0	145.0
β	60.9	65.8	66.8	67.8	68.8	69.8	70.8	71.8	72.8	73.8	74.8	75.8	76.8	77.8	78.8
α	269.9	272.7	273.2	273.7	274.1	274.5	274.8	275.1	275.4	275.7	275.9	276.0	276.1	276.1	276.1
δ	37.4	42.4	43.5	44.5	45.5	46.5	47.6	48.6	49.6	50.6	51.7	52.7	53.7	54.7	55.7
V_g	17.3	18.3	18.5	18.7	18.8	19.0	19.2	19.4	19.6	19.8	20.0	20.2	20.4	20.5	20.7
λ_s	144	145	146	147	148	149	150	151	152	153	154	155	160		
$\lambda - \lambda_s$	145.0	145.1	145.1	145.1	145.1	145.2	145.2	145.3	145.5	145.9	149.9	323.3	324.7		
β	79.8	80.8	81.8	82.8	83.8	84.8	85.8	86.8	87.8	88.8	89.8	89.2	84.3		
α	276.1	275.9	275.7	275.4	275.0	274.5	273.9	273.2	272.4	271.4	270.3	269.1	259.9		
δ	56.8	57.8	58.8	59.8	60.7	61.7	62.7	63.6	64.6	65.5	66.4	67.2	71.0		
V_g	20.9	21.1	21.3	21.5	21.7	21.9	22.1	22.2	22.4	22.6	22.8	23.0	23.9		

Table 7 – The yearly numbers of meteors classified as AXD. EDMOND data in 2004 is incorrect (see Table 3).

Year	EDMOND	SonotaCo	CAMS
2004	19		
2005	0		
2006	0		0
2007	1	21	33
2008	5	2	23
2009	1	7	68
2010	8	7	128
2011	22	7	40
2012	29	9	46
2013	40	8	
2014	67	2	
2015	27	6	
2016	50	7	
2017		3	
2018		9	
Total	269	88	338

4 Discussion

It is necessary to note that the three video data sets have peculiar partialities; SonotaCo net observations missed the 2014 maximum, EDMOND's depend almost entirely on 2014 observations and CAMS' 2007 observations are partial with an overwhelming majority in 2010 though the reason is not known.

We cannot determine the exact maximum of KCG because of these partialities. SonotaCo net data suggest two peaks at $\lambda_s = 141$ and at $\lambda_s = 145$, EDMOND also at $\lambda_s = 140$ and at $\lambda_s = 144$, but CAMS a single maximum at $\lambda_s = 141$. These differences might be caused by the fluctuation of the activity itself, though observations are significantly biased. Care is necessary not to be under a preconceived impression of when the maximum occurs.

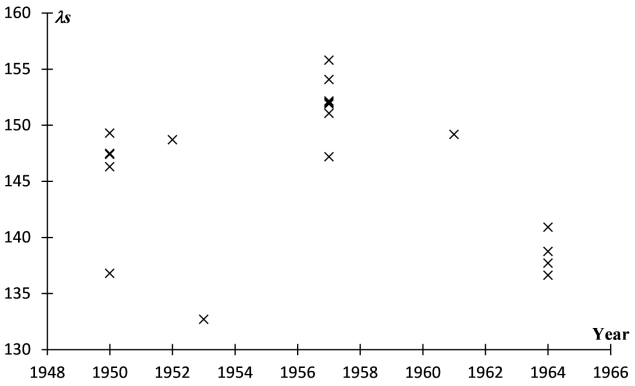

Figure 6 – Observed λ_s distribution of 19 photographic meteor KCG candidates with year.

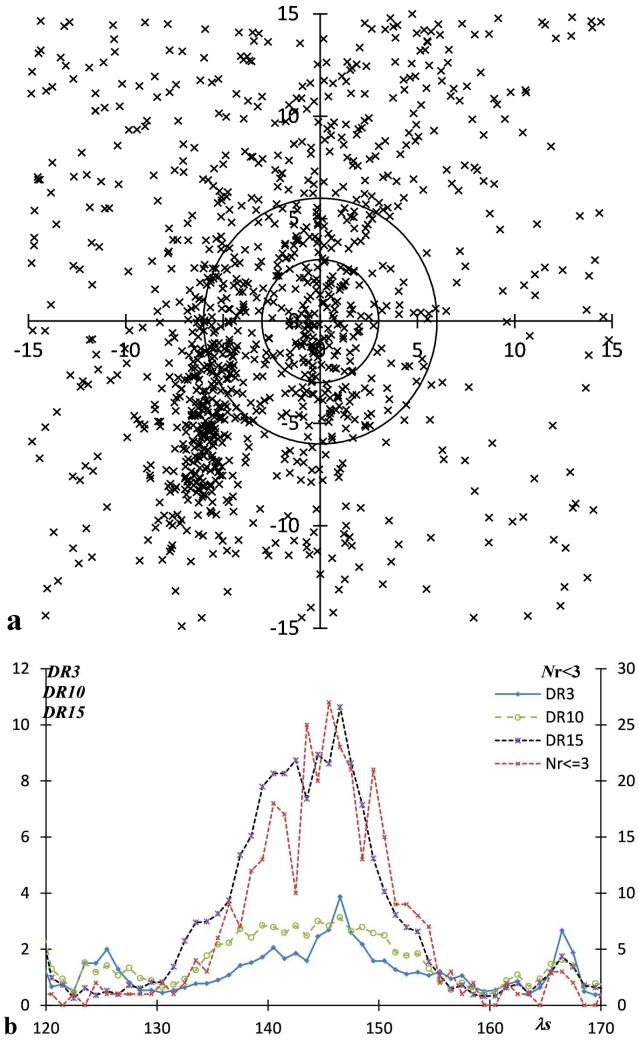

Figure 7 – Results of the iteration for AXD using EDMOND data. a: compensated radiant distribution; y-axis runs through $\lambda - \lambda_s = 146.6$. b: activity profiles based on data compensated for radiant drift. Detailed explanations are same as Figure 3.

Table 8 – The radiant estimation for ZDR estimated from EDMOND iteration results.

λ_s	140	145	146	147	148	149	150	151	152	153	154	155	156	157	158
$\lambda - \lambda_s$	191.0	180.4	175.7	168.9	158.5	142.1	118.2	92.3	72.7	60.0	51.9	46.5	42.7	39.9	37.7
β	74.3	81.5	82.9	84.2	85.4	86.3	86.8	86.6	85.8	84.7	83.4	82.1	80.7	79.3	77.8
α	295.2	284.5	281.8	279.0	276.0	272.9	269.8	266.5	263.3	260.1	256.9	253.8	250.8	248.0	245.3
δ	56.2	60.9	61.6	62.2	62.7	63.1	63.3	63.4	63.4	63.3	63.1	62.7	62.2	61.6	60.9
V_g	25.2	23.8	23.5	23.2	22.9	22.6	22.3	22.0	21.8	21.5	21.2	20.9	20.6	20.3	20.0
λ_s	159	160	161	162	163	164	165								
$\lambda - \lambda_s$	36.0	34.6	33.4	32.5	31.7	31.0	30.3								
β	76.4	74.9	73.4	71.9	70.4	69.0	67.5								
α	242.8	240.4	238.2	236.2	234.4	232.8	231.2								
δ	60.2	59.3	58.3	57.3	56.2	55.0	53.8								
V_g	19.8	19.5	19.2	18.9	18.6	18.3	18.0								

Table 9 – The yearly numbers of meteors classified as ZDR. EDMOND data in 2004 is incorrect (see Table 3).

Year	EDMOND	SonotaCo	CAMS
2004	14		
2005	0		
2006	0		0
2007	0	2	14
2008	1	1	16
2009	6	11	18
2010	8	14	42
2011	29	3	22
2012	22	15	57
2013	12	7	
2014	45	1	
2015	41	1	
2016	85	2	
2017		7	
2018		5	
Total	263	69	169

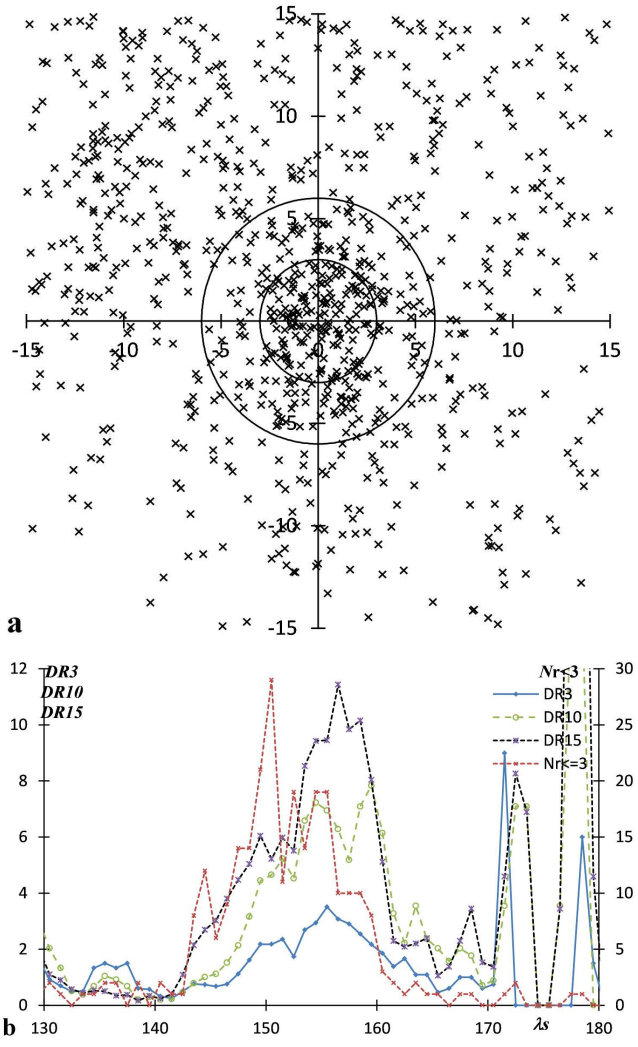

Figure 8 – Results of the iteration for ZDR using EDMOND data. a: compensated radiant distribution; y-axis runs through $\lambda - \lambda_s = 47.5$. b: activity profiles based on data compensated for radiant drift. Detailed explanations are same as Figure 3.

It is worthwhile to note that the orbits of KCG, AXD and ZDR have a unique peculiarity; their semi-major axis remains almost constant near $a = 2.5$–3.0 au during their activity period (Figure 9), though their perihelion coordinates (λ_Π, β_Π) move rather rapidly. Future observations, especially next year in 2021, would reveal the details of their origin and whether these three streams have a common origin.

References

Jenniskens P., Nénon Q., Albers J., Gural P. S., Haberman B., Holman D., Morales R., Grigsby B. J., Samuels D., and Johannink C. (2016). "The established meteor showers as observed by CAMS". *Icarus*, **266**, 331–354.

Kornoš L., Koukal J., Piffl R., and Tóth J. (2014a). "EDMOND meteor database". In Gyssens M., Roggemans P., and Żołądek P., editors, *Proceedings of the International Meteor Conference, Poznań, Poland, 22–25 August, 2013*. IMO, pages 23–25.

Kornoš L., Matlovič P., Rudawska R., Tóth J., Hajduková Jr. M., Koukal J., and Piffl R. (2014b). "Confirmation and characterization of IAU temporary meteor showers in EDMOND database". In Jopek T. J., Rietmeijer F. J. M., Watanabe J., and Williams I. P., editors, *Meteoroids 2013, Proceedings of the International Conference held at the Adam Mickiewicz University, Poznań, Poland, Aug. 26-30, 2013*. A. M. Univ. Press, pages 225–233. (see also

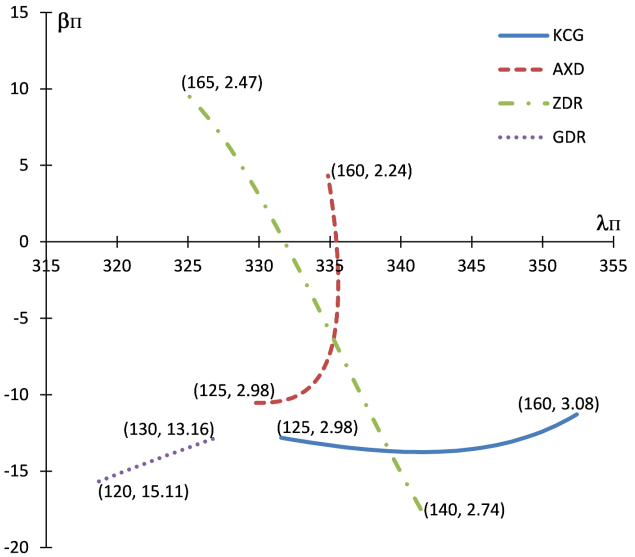

Figure 9 – The shift of perihelia in ecliptic latitude β_Π and longitude λ_Π of CDC members in EDMOND data. Each line is estimated from observations over the period shown in Table 1 and lines are extended at both ends; the longitudes of the Sun λ_s and the semi-major axes a are given in the parentheses as (λ_s, a). The two ends of each line do not mean the start and the end of the activities; they represent the extension.

"EDMOND", `https://fmph.uniba.sk/en/microsites/daa/division-of-astronomy-and-astrophysics/research/meteors/edmond/`).

Koseki M. (2009). "Meteor shower records: A reference table of observations from previous centuries". *WGN, Journal of the IMO*, **37:5**, 139–160.

Koseki M. (2014). "Various meteor scenes II: Cygnid-Draconid Complex (κ-Cygnids)". *WGN, Journal of the IMO*, **42:5**, 181–197.

Koseki M. (2019). "Profiles of meteor shower activities inferred from the radiant Density Ratios (DR)". *WGN, Journal of the IMO*, **47:6**, 168–179.

SonotaCo (2009). "A meteor shower catalog based on video observations in 2007–2008". *WGN, Journal of the IMO*, **37:2**, 55–62. (see also "SonotaCo Network Simultaneously Observed Meteor Data Sets", `http://sonotaco.jp/doc/SNM/`).

Whipple F. L. (1954). "Photographic meteor orbits and their distribution in space". *Astron. J.*, **59**, 201–217.

Handling Editor: David Asher

Conferences

Special issue of WGN: IMC 2020

Cis Verbeeck[1]

When the COVID pandemic ruined the plans to have the IMC 2020 in Hungary, the IMO Council and the LOC and SOC decided to organize a 1-day online IMC 2020 instead, on Saturday September 19. It is my pleasure to present this special "IMC 2020" issue to you, full of IMC 2020 Proceedings papers.

Seamlessly hosted by and utilizing the Zoom service of the LOC (Research Centre for Astronomy and Earth Sciences in Hungary), the online IMC reached 96 registered participants joining the IMC from different time zones (23 countries). Though obviously the program was much shorter this year, it still covered most of the main topics of meteor science, and from first impressions it seems that people agree with my personal feeling that the meeting was a great success.

Of course an online IMC does not provide all the benefits of in-person meetings, but it brought the participants into contact with other people and their work, which was very welcome one year after the previous IMC, especially in this pandemic age. Going virtual also opened an opportunity for IMO to reach a new, wider audience, tearing down the financial and travel restrictions that refrain part of the meteor community to attend the regular IMCs.

Having had a virtual IMC, we can consider to have more virtual IMCs, either as part of physical IMCs or alternating with them at whichever timescale. The results of the IMC 2020 satisfaction survey will be an important input for related policies.

Meanwhile, enjoy reading this issue, and stay tuned for more IMC 2020 Proceedings papers in the December issue of WGN!

[1]Royal Observatory of Belgium, Ringlaan 3, 1180 Brussels, Belgium. Email: cis.verbeeck@oma.be

IMO bibcode WGN-485-verbeeck-imc2020 NASA-ADS bibcode 2020JIMO...48..138V

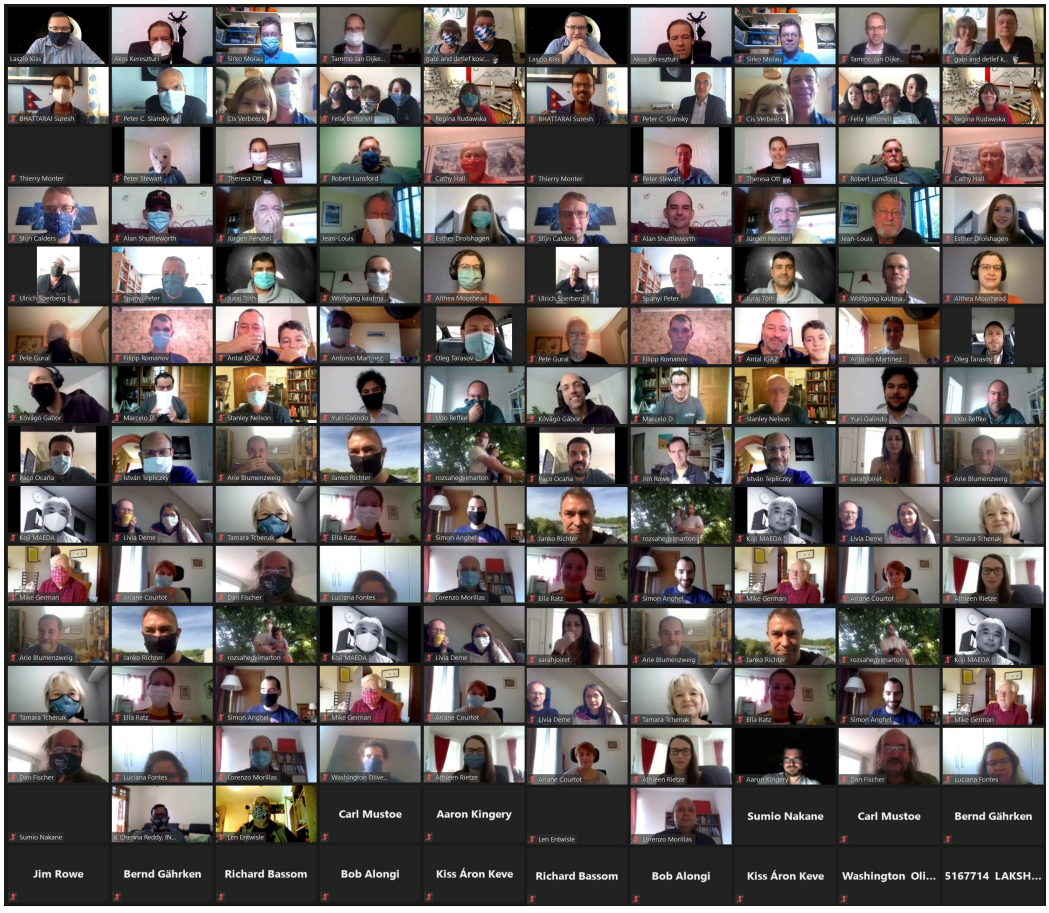

Figure 1 – "Group picture" of the IMC 2020 participants.

Table 1 – The IMC 2020 programme

10:00-10:15	Opening Talk	Cis Verbeeck
	SESSION 1 – Meteor observation Networks	
10:15-10:25	The AllSky7 Fireball Network Germany	Sirko Molau
10:30-10:40	Year-to-year comparison of BRAMS forward scatter observations of selected meteor showers	Cis Verbeeck, Hervé Lamy, Stijn Calders, Antonio Martínez Picar, Antoine Calegaro, Michel Anciaux
	SESSION 2 – Meteor Shower updates	
10:45-10:55	Update on the ongoing chi Cygnid meteor shower	Peter Jenniskens
	SESSION 3 – Outreach and special events	
11:00-11:10	Meteor Shower as key for Astronomy Outreach in Nepal	Suresh Bhattarai
11:15-11:25	Fake news vs Fake Fireballs (Miscellaneous session)	Regina Rudawska
11:30-11:40	Another Daylight Fireball over The Netherlands: the event of August, 25, 2020	Felix Bettonvil
11:45-11:58	Noctilucent clouds over Munich in July 2020	Peter C. Slansky
12:00-12:05	Group Photo... turn your camera on!	
12:05-13:00	Break - European lunch break	
	SESSION 4 – Meteor physics	
13:00-13:10	A study on latitudinal and altitudinal asymmetry in diurnal variation of sporadic meteor flux	Chenna Reddy Kammadhanam
13:15-13:25	The luminous efficiency determination and its difficulties	Esther Drolshagen, Theresa Ott
13:30-13:40	Connecting ionospheric, optical, infrasound and seismic data from meteors in Hungary	Akos Kereszturi, Veronika Barta, István Bondár, Csenge Czanik, Antal Igaz, Péter Mónus, Bernadett Pál
13:45-13:55	A renewed discussion: The Hyperbolic Meteors and its Interestellar Origin	Marcelo De Cicco
14:00-14:10	Does a meteor's "color" reflect its composition?	Althea Moorhead
14:15-14:25	Meteor Energy Obtainable from Acoustic Data	Luke McFadden
	SESSION 5 – Meteor showers	
14:30-14:40	Enhanced Aurigid activity 2019 and predictions for 2021	Jürgen Rendtel, Esko Lyytinen and Jeremie Vaubaillon
14:45-14:55	Upcoming Eta-Aquariid outbursts	Auriane Egal
	POSTERS SESSION	
15:00-15:10	Poster pitch session:	
	Lyrids 2020 observations by AMOS, spectral, visual and photographic methods	J. Tóth, P. Matlovič, P. Zigo, L. Kornoš, J. Šimon, T. Paulech, M. Baláž, A. Pisarčíková, D. Žilinská, D. Bartková, J. Dudík and S. Kaniansky
	Using a night vision device for video recording Perseids 2019	Oleg Tarasov, Kirill Moskvin
15:15-15:55	Coffe Break	
	SESSION 6 – Meteor detection software	
16:00-16:10	Filtering False Positives from Meteor Surveillance Images with Deep Learning	Galindo Yuri Oliveira
16:15-16:25	Impact of Starlink on meteor detection algorithms	Pete Gural
16:30-16:40	Monitor Exoss: Dashboard Panel for Meteor Monitoring Network On Time	Negri Guilherme, Rescigno, Giovanni; Negri, Guilherme; Souza, Warley; Mastria, Marco; De Cicco, Marcelo; Exoss Team
16:45-16:55	MALBEC: Optimization of mobile double station meteor observation	Athleen Rietze, Jérémie Vaubaillon, Danica Zilkova
	SESSION 7 – Meteor research groups	
17:00-17:10	Status of ESA's Meteor Research Group	Detlef Koschny
17:15-17:25	Meteor Research at Western University	Peter Brown
17:30-17:40	The Global Meteor Network – overview	Denis Vida
17:45-18:00	Closing Talk	Cis Verbeeck

Experiencing two different and unique versions of IMC

Suresh Bhattarai[1]

This paper is a reflection of my experience attending two International Meteor Conferences in completely differently settings. It explains how I felt attending this conference in 2010 in person in Armagh, Northern Ireland (UK) and virtually this year. In this paper, I outline my experiences of both types of meeting format.

Received 2020 October 6

Introduction

Just as astronomy is fascinating to many people, it has also been one of my favorite subjects. In fact, I always find astronomy to be more than just science, it's also art as it gives you an opportunity to imagine the craziest things at the same time as deeply as the possible. When we started Nepal Astronomical Society (NASO) in 2007, meteor shower observing was the first thing that we decided to carry out for our outreach efforts. The Perseid Meteor Shower 2007 marked the start of our journey of regularly observing meteor shower activity in a standard way.

There is some connection with my interest into astronomy and meteor activity. I used to visit temple with my mother during early morning and one of the fine days we both saw a very bright object in the sky. At the time, I did not know what I had seen, but I was so fascinated to find out and that started me doing astronomy. I don't recall exactly the date but it was the beginning of my astronomical journey. When I was studying bachelors of science at Tri-Chandra Campus, we used to have discussions about what is out there, why we are here, etc among friends. As a result, an informal group formed with a name as Student Astronomical Society (SAS) in June 2007 which later on August 6, 2007 got a new name as Nepal Astronomical Society (NASO) and we were joined by some faces with experience from the astronomy outreach community such as Dr. Rishi Shah, Academician at Nepal Academy of Science and Technology (NAST). As we were looking for guardianship, he agreed our proposal to guide us as our first president. It was in 2014 when he told me that I was ready for leadership of the group hence requested me to step up from secretary to president and register the group officially.

In 2010, I got an opportunity to attend International Meteor Conference (IMC) as EurAstro Association from Germany and International Meteor Organization (IMO) decided to provide financial support. This year, it happened that due to COVID-19, IMO decided to host online version of the IMC which was made freely available. As a result, I got an opportunity to attend the meeting, present our works in meteor astronomy outreach and network with experts from the field. In both years, I had my best time learning from the IMC.

Attending IMC2010

IMC2010 was special for many reasons which helped us to decide to attend. One of the main reasons was the Human Orrery which is hosted at the Armagh Observatory. One of the reasons of mine attending the IMC2010 was to field visit the Human Orrery and then build some in Nepal. It went as planned and although we did set up an improvised version at one of the schools in Kathmandu but this did not last long. We tried to build one as we saw in Armagh but we lacked resources for that and hence our idea of implementing human Orrery in many parts of the country remains in a wish list.

One of the best experiences that I had during IMC2010 was pre-conference workshop on Fireball. I had an opportunity interact, share and learn from many experts in the field from ESA, NASA, etc. The main conference was another great experience. I will not forget the time when I missed the group photo as I woke up late due to the failure of my alarm clock at accommodation! I did a presentation on how we were doing meteor astronomy outreach in Nepal and it was a great experience.

In 2009, I was I touch with Dr. Prakash Atreya as he along with his team planned trip to Nepal for Leonid Outburst. I had an opportunity to coordinate him and his team for their Nepal tour and guide them to the respective government offices for the observational settings. If I remember, this might be the first time I came to know about Human Orrery at Armagh Observatory as Dr. Atreya was doing PhD there at that time.

The best part of the IMC informal settings where you feel more comfortable to interact with people and network. The social networking sessions, which included singing, poem recitation, etc. were excellent. All, I remember now quickly if someone asked me about IMC is how I wrote a poem on Meteor and recited that in front of everyone. I remember the Turner bar where I sang a song and the theatre where I watched a movie!

We had a fireball sighting over Nepal in March 2020 and my attendance in IMC2020 helped me greatly to solve the people's concern about the event as I could email people I met in the conference and asked for their help to verify whether that incident was fireball or not. Though the information from the people in the network

[1]Nepal Astronomical Society (NASO), PO Box 3649, Kathmandu, Nepal. Email: suresh@nepalastronomicalsociety.org

IMO bibcode WGN-485-bhattarai-imc2020 NASA-ADS bibcode 2020JIMO...48..140B

did not work, it was certainly a motivation to look into it and confirm that the fireball had not fallen in Nepal, at least in populated area. It most likely fell in Tibet, China.

Attending IMC2020

IMC2020 was a new experience to me as it was for everyone attending it via zoom. Though the meeting did not have a quality of original IMC such as I explained earlier, it has certainly provided an opportunity to attend and network for the people like me who could not attend the meeting otherwise due to financial constraint. It was due to this constraint that was unable to attend IMC for so many years despite of strong interest to attend it due to its lively nature and fun attending.

Though the socialization part was missing in online version, networking session worked very well as we had different rooms where we could go to and interact with people. I found it to be one of the impressive aspects of the online version making online IMC very close to the onsite IMCs.

Conclusion

With an experience of attending both onsite and online versions of the IMCs in 2010 and 2020 respectively, I strongly feel that IMO should either organise these events separately or together allowing more people to participate. It will enable people like me to be a part of IMC and IMO sharing our work and contributing to the IMO community without much financial burden.

Recommendation

I request that the IMO organize such events regularly as these provide an opportunity for people like us to attend the meeting without financial constraint. Financial constraint was the main reason that I could not return to the IMC despite the event's very strong impression on me and my activities in Nepal.

Acknowledgement

I would like to express my sincere gratitude to late Jean-Luc Digaye who supported my travel to IMC2010. I would also like to thank Dr. Rishi Shah for the encouragement. I would also like to express my sincere thanks to Ms. Manisha Dwa, project coordinator at Nepal Astronomical Society (NASO) for her photographs her support which helped make my participation a success.

Year-to-year comparison of BRAMS forward scatter observations of selected meteor showers

Cis Verbeeck[1], *Hervé Lamy*[2], *Stijn Calders*[2], *Antonio Martínez Picar*[1], *Antoine Calegaro*[2], *and Michel Anciaux*[2]

The BRAMS network consists of a dedicated forward scatter beacon and about 30 forward scatter receiving stations located in or near Belgium. Though these stations perform observations all year round, we still need the help of citizen scientists from the Radio Meteor Zoo for accurate detection of complex overdense meteor echoes observed during meteor showers. From 2016 onwards, we organized Radio Meteor Zoo campaigns for the major showers. Here, we perform a year-to-year comparison of BRAMS activity curves for selected showers in the years 2016–2019. Our estimate of the diurnal variation of the sporadic background is consistent from year to year, with a maximum in the early local morning hours. We find that the peaks in estimated shower activity in different years do not correspond to the same interval in solar longitude but that they do nicely align as diurnal patterns. This is an indication that the diurnal variation of the sensitivity of the system (i.e., the Observability Function) is the dominant factor in our observations.

Received 2020 October 13

This work has been presented at the International Meteor Conference 2020 (held online).

1 Introduction

BRAMS (Belgian RAdio Meteor Stations) is a radio network located in Belgium using forward scatter measurements to detect and characterize meteoroids. It consists of one dedicated transmitter located in Dourbes in the south of Belgium and approximately 30 receiving stations spread all over the Belgian territory. The transmitter emits a circularly polarized continuous wave (CW) at a frequency of 49.97 MHz and with a power of 130 W. All receiving stations use the same material (including a 3 elements Yagi antenna) and are synchronized using GPS clocks. More details can be found in, e.g., (Lamy et al., 2015).

Each BRAMS receiving station is recording continuously, producing each day 288 WAV files and detecting about 1500–2000 meteors. Though significant advances in automatic detection of meteor reflections in the BRAMS spectrograms have been made, the best detector is still the human eye. In August 2016, the Radio Meteor Zoo[b] was launched. This citizen science project, hosted on the Zooniverse platform (Lintott et al., 2008), exploits the (trained) human eye of many volunteers for classifying meteor reflections during certain observing campaigns. This enabled the BRAMS team to publish the present shower activity results. More information about the Radio Meteor Zoo can be found in (Calders et al., 2016) and (Calders et al., 2017).

[1]Royal Observatory of Belgium, Ringlaan 3, 1180 Brussels, Belgium.
cis.verbeeck@oma.be and antonio.martinez@oma.be

[2]Royal Belgian Institute of Space Aeronomy, Ringlaan 3, 1180 Brussels, Belgium.
herve.lamy@aeronomie.be, stijn.calders@aeronomie.be, antoine.calegaro@aeronomie.be and michel.anciaux@aeronomie.be

IMO bibcode WGN-485-verbeeck-brams
NASA-ADS bibcode 2020JIMO...48..142V

[b]http://www.radiometeorzoo.org

In the current paper, we compare meteor shower activity profiles from BRAMS observations (receiving station: Humain, code BEHUMA) of the Geminids and Perseids in 2016–2019. Section 2 compares our estimation of the sporadic background around the activity period of the Geminids in 2016–2019, while Sections 3 and 4 compare the BRAMS activity curves near the maximum period of respectively Geminids and Perseids in the years 2016–2019. Conclusions are outlined in Section 5.

2 Estimated sporadic background near the Geminid activity period: comparison 2016–2019

With the current set-up of the BRAMS stations, it is not yet possible to identify the shower (or sporadic background) of a specific meteor reflection. In order to estimate the sporadic background during shower observations, a sine curve is fitted to the average of the observed diurnal hourly rates of meteor echoes over a few (2 to 4) days well outside the main shower activity. This sine curve is then subtracted from the hourly total number of meteor reflections to yield an estimate of the hourly number of shower meteors. This approach was described in detail in (Verbeeck et al., 2017).

Figure 1 provides a year-to-year (2016–2019) comparison of the average of the observed diurnal hourly rates of meteor echoes over a few days well outside the main Geminid activity (left panel), and of the weighted sine fits of these average curves (right panel). Looking at the error bars in the 2016 curve, we see that there is a considerable spread between the observed diurnal rates in the individual sporadic days from which the average was calculated. This means that our estimates of the sporadic background can be only rough approximations. We also note that the observed average diurnal hourly rates are well-described by a weighted sine fit, and that the diurnal maximum takes place in the early local morning hours, as expected from apex considerations (Powell, 2017).

Comparing the estimated sporadic background around the Geminid activity period in 2017–2019, we

see similar rates and sine fits from year to year. In 2016, the shape is similar, but the error bars are larger and the observed levels are about 25% higher than in 2017–2019. Probably the error bars are larger in 2016 because the sporadic background was averaged over only 2 days (December 5 and 16), as opposed to 3 days in 2017 and 2018 (December 2, 3 and 18) and 4 days in 2019 (December 9, 10, 17, and 18). The higher estimated sporadic background level in 2016 can perhaps be attributed to contamination from the Geminids (having considered December 16 instead of December 18 as a non-shower day).

3 Geminids 2016–2019

Figure 2 shows the estimated hourly number of Geminid reflections in 2016–2019, obtained by subtracting the estimated diurnal sporadic activity from the hourly total number of meteor reflections.

The peaks in estimated shower activity in different years do not correspond to the same interval in solar longitude (see the left panel in Figure 2). The right panel in Figure 2 clearly shows that the peaks in estimated shower activity do nicely align as diurnal patterns.

Since the number of observed shower meteors is the product of the real number of shower meteors and the sensitivity of the system, it is clear from these results that the sensitivity of the system is the dominant factor. Due to its dependence on the radiant position in the sky, the system sensitivity has a diurnal pattern, called the Observability Function (OF, (Verbeeck, 1997)).

Since we know that the hourly total number of meteor reflections is dominated by the large number of reflections by faint (mostly sporadic) underdense meteors (Verbeeck et al., 2017), we also analyze the meteor reflections lasting at least 10 seconds, which are dominated by shower meteor reflections. Figure 3 shows the estimated hourly number of Geminid reflections lasting at least 10 seconds in 2016–2019. We observe the same trend as in Figure 2: the peaks in estimated shower activity in different years do not correspond to the same interval in solar longitude but they do nicely align as diurnal patterns.

4 Perseids 2016–2019

Figure 4 shows the estimated hourly number of Perseid reflections lasting at least 10 seconds in 2016–2019.

As was the case for the Geminids, we observe that the peaks in estimated shower activity in different years do not correspond to the same interval in solar longitude (see the left panel in Figure 4) but do nicely align as diurnal patterns as seen in the right panel in Figure 4.

5 Conclusions

Employing the Radio Meteor Zoo detections of meteor reflections from forward scatter observations from the BRAMS receiving station at Humain, we have estimated the sporadic background and subtracted it from the total radio meteor activity to obtain an estimate of the shower activity around the maximum of the Geminids and Perseids in 2016–2019.

In order to estimate the sporadic background during shower observations, we fit a sine curve to the average of the diurnal hourly rates of meteor echoes over a few (2 to 4) days well outside the main shower activity. Though there is a large scatter in the observed diurnal hourly rates of meteor echoes on individual "sporadic" days, the average diurnal curve and the sine fit are consistent from year to year, with a maximum in the early local morning hours. Comparing the estimated sporadic background around the Geminid activity period in 2017–2019, we see similar rates and sine fits from year to year. In 2016, the shape is similar, but the error bars are larger and the observed levels are about 25% higher than in 2017–2019. This difference can possibly be attributed to the fact that in 2016, the sporadic background was averaged over only 2 days, of which one (December 16) was close to the Geminid maximum (hence, prone to contamination from the Geminids).

Comparing the estimated shower activity from year to year, we find for all considered cases (all Geminid reflections, Geminid reflections lasting at least 10 s, Perseid reflections lasting at least 10 s) that the peaks in estimated shower activity in different years do not correspond to the same interval in solar longitude (see, e.g., the left panel in Figure 2) but that the shower peaks do nicely align as diurnal patterns (see, e.g., the right panel in Figure 2).

Since the number of observed shower meteors is the product of the real number of shower meteors and the sensitivity of the system, it is clear from these results that the sensitivity of the system is the dominant factor. Due to its dependence on the radiant position in the sky, the system sensitivity has a diurnal pattern, called the Observability Function (OF, (Verbeeck, 1997)). So to get an estimate of the real number of shower meteors, we have to calculate or estimate the OF. This is under development.

Acknowledgements

The BRAMS network is a project from the Royal Belgian Institute for Space Aeronomy and funded by the Solar-Terrestrial Center of Excellence (STCE). The authors thank all volunteers who helped us with the classification of the spectrograms. These volunteers make the success of the Radio Meteor Zoo. We also thank the Zooniverse team, who are hosting the Radio Meteor Zoo and who are always very enthusiastic in supporting us. Last but not least, we want to thank all volunteers who host a BRAMS receiving station. Their assistance is of course essential to the BRAMS project. The authors are grateful for their constant support.

References

Calders S., Lamy H., Martínez Picar A., Tétard C., Verbeeck C., and Gamby E. (2017). "The Radio Meteor Zoo: involving citizen scientists in radio meteor research". In Gyssens M., Pavlović D., and Rault J.-L., editors, *Proceedings of the Interna-*

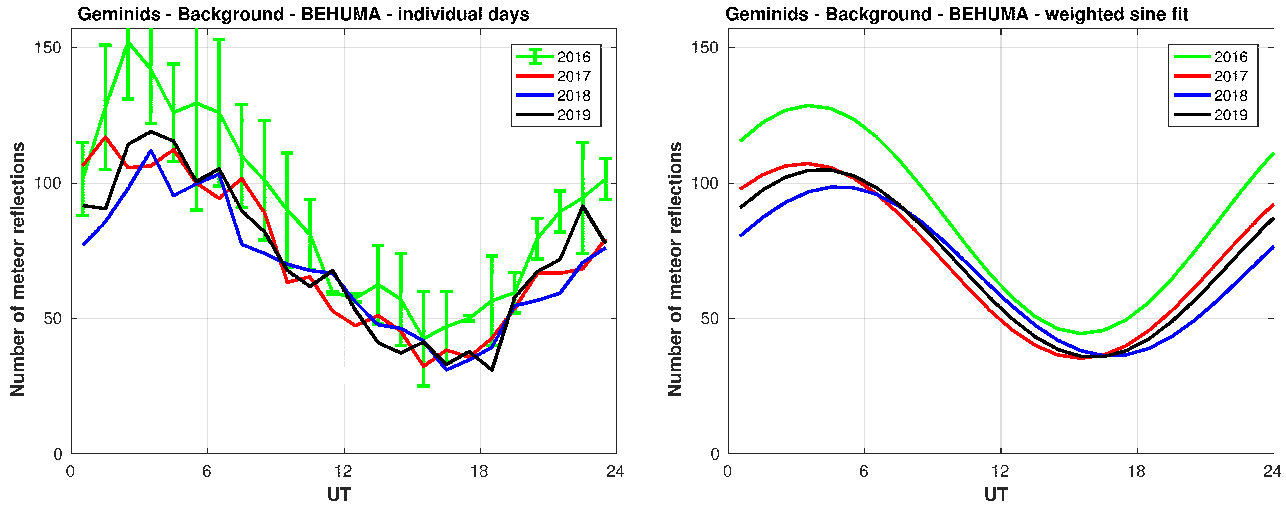

Figure 1 – Left: the average of the observed diurnal hourly rates of meteor echoes over a few days well outside the main Geminid activity, for the years 2016–2019. The error bars (standard deviation of rates observed in individual days) are plotted for the 2016 curve. *Right:* the weighted sine fits to these observed average diurnal hourly rates of meteor echoes.

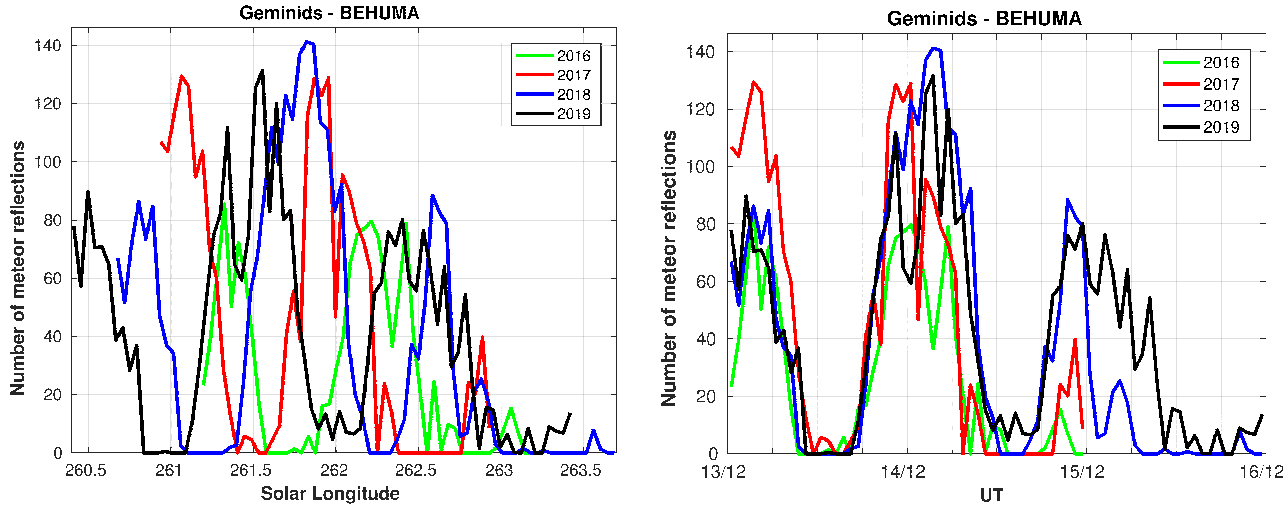

Figure 2 – Left: the estimated hourly number of Geminid reflections in 2016–2019, expressed as a function of solar longitude (J2000). *Right:* the estimated hourly number of Geminid reflections in 2016–2019, expressed as a function of day and time (UT).

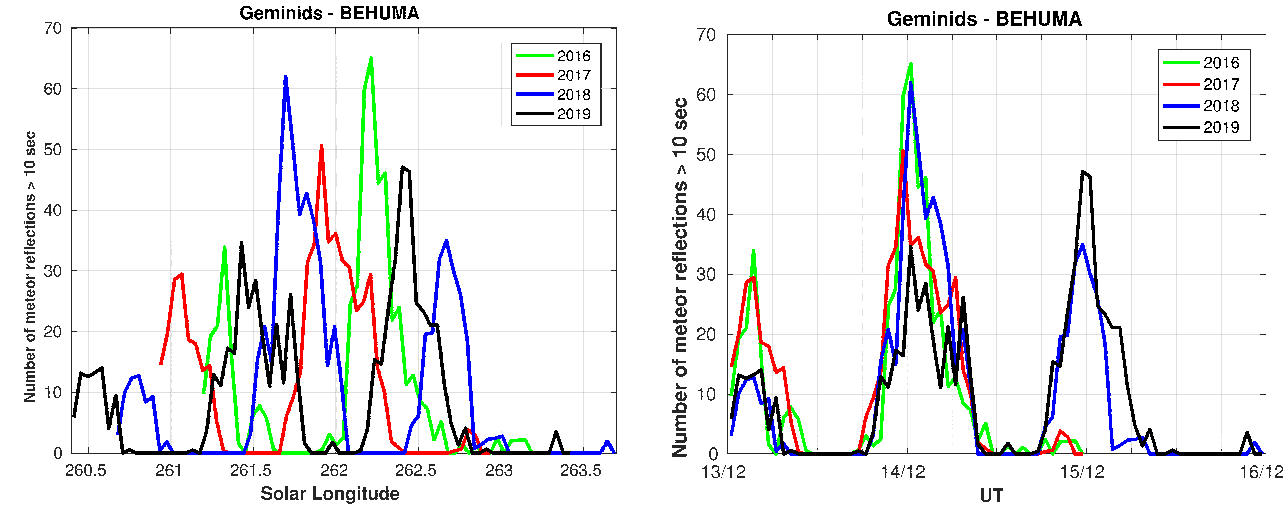

Figure 3 – Left: the estimated hourly number of Geminid reflections lasting at least 10 seconds in 2016–2019, expressed as a function of solar longitude (J2000). *Right:* the estimated hourly number of Geminid reflections lasting at least 10 seconds in 2016–2019, expressed as a function of day and time (UT).

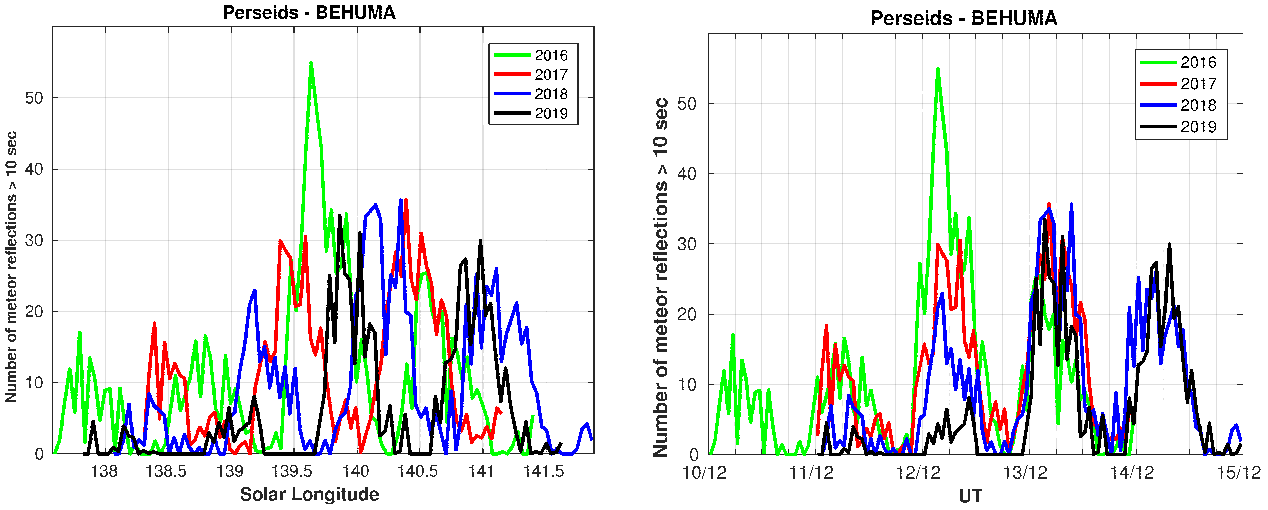

Figure 4 – Left: the estimated hourly number of Perseid reflections lasting at least 10 seconds in 2016–2019, expressed as a function of solar longitude (J2000). *Right:* the estimated hourly number of Perseid reflections lasting at least 10 seconds in 2016–2019, expressed as a function of day and time (UT).

tional Meteor Conference, Petnica, Serbia, 21–24 September 2017. IMO, pages 13–15.

Calders S., Verbeeck C., Lamy H., and Martínez Picar A. (2016). "The Radio Meteor Zoo: a citizen science project". In Roggemans A. and Roggemans P., editors, *Proceedings of the International Meteor Conference,* Egmond, The Netherlands, 2–5 June 2016. IMO, pages 46–49.

Lamy H., Anciaux M., Ranvier S., Calders S., Gamby E., Martínez Picar A., and Verbeeck C. (2015). "Recent advances in the BRAMS network". In Rault J.-L. and Roggemans P., editors, *Proceedings of the International Meteor Conference,* Mistelbach, Austria, 27–30 August 2015. IMO, pages 171–175.

Lintott C. J., Schawinski K., Slosar A., Land K., Bamford S., Thomas D., Raddick M. J., Nichol R. C., Szalay A., Andreescu D., Murray P., and Vandenberg J. (2008). "Galaxy Zoo: Morphologies derived from visual inspection of galaxies from the Sloan Digital Sky Survey". *Monthly Notices of the Royal Astronomical Society*, **389**, 1179–1189.

Powell C. (2017). "Modelling & analysis of diurnal variation in meteor flux". *WGN, Journal of the IMO*, **45:2**, 32–37.

Verbeeck C. (1997). "Calculating the sensitivity of a forward scatter setup for underdense shower meteors". In Knöfel A. and Roggemans P., editors, *Proceedings of the International Meteor Conference,* Apeldoorn, The Netherlands, 19-22 September 1997. IMO, pages 122–132.

Verbeeck C., Lamy H., Calders S., Tétard C., and Martínez Picar A. (2017). "Overview of major shower observations 2016–2017 by the BRAMS network". In Gyssens M., Pavlović D., and Rault J.-L., editors, *Proceedings of the International Meteor Conference,* Petnica, Serbia, 21–24 September 2017. IMO, pages 138–144.

Handling Editor: Jean-Louis Rault

This paper has been typeset from a LaTeX file prepared by the authors.

The 2020 Chi-Cygnids

Peter Jenniskens[1]

The 2020 return of the Chi-Cygnid meteor shower (IAU #757) is documented as observed by the CAMS low-light camera networks this year. 449 meteors are identified as likely shower members. The shower was active from August 5 to September 25, with a maximum on September 13–18 (solar longitude 171°–176°). The activity profile was skewed, with a gradual rise and an abrupt end. During that time, the radiant drifted to lower sun-centered ecliptic longitude and higher ecliptic latitude. Orbital elements show a gradual increase of the perihelion distance and inclination with solar longitude, while the semi-major axis and longitude of perihelion of the orbits remained constant. Asteroid 2020 RF may be related to the stream, but that is not certain.

Received 2020 October 13

This work has been presented at the International Meteor Conference 2020 (held online).

1 Introduction

In late August 2020, the CAMS meteoroid orbit survey flagged a few meteors as χ-Cygnids (IAU shower 757), a Jupiter-family comet type shower that had not been seen since 2015. In 2015, Martin Breukers and Carl Johannink first noticed this new shower in CAMS BeNeLux low-light video data and they were later seen by visual observers as well (Jenniskens, 2015; Roggemans et al., 2015; Koukal et al., 2016).

If these August meteors heralded a return of the χ-Cygnids, a nice outburst of slow meteors had just started and might continue during much of September (Jenniskens et al., 2020; Jenniskens, 2020). However, the orbital elements were very different during this early sighting than in late September at the peak, when the shower radiant is near the star χ Cygni. Several other showers were identified at nearby positions, but they have different longitude of perihelion and do not appear to be related (Rudawska & Jenniskens, 2014; Jenniskens, 2020).

Here, we report on observations of this χ-Cygnid shower by the various CAMS networks (Table 1) in the weeks following that first detection. The shower manifested much as anticipated. CAMS BeNeLux was again most successful in capturing this high northern latitude shower.

2 Methods

The Cameras for Allsky Meteor Surveillance (CAMS) project is a group of international networks of about 548 low-light video cameras that triangulate the trajectories of visible +5 to −5 magnitude meteors. The camera video feed is analyzed by software modules built by Pete Gural, in an automated video-surveillance like manner thanks to scripts by Dave Samuels and Steve Rau (Jenniskens et al., 2011). The number of participating CAMS networks has gradually increased over the years, with a big expansion on the southern hemisphere being completed in 2019. 176 cameras were added, resulting in a rapid increase of the number of triangulated meteors to over a thousand a day on average. As a result, unusual meteor showers are now reported about once every one or two months.

To obtain its shower association, each radiant and speed are compared to a look-up table of past identified showers, which are shown by colours representing speed (red is fast, blue is slow). The measured radiant positions are displayed at the website `http://cams.seti.org/FDL/`. When using this website, first choose a network and a date to view the data.

3 Results

Figure 1 shows the detection of the χ-Cygnids on 2020 August 18, a grouping of blue-coloured (slow-moving) meteors between the constellations of Aquila and Delphinus. The slow late α-Capricornids (IAU #692, ε-Aquariids) and late κ-Cygnids (197, August Draconids) are also shown as blue points. The radiant of the χ-Cygnids is significantly displaced from that of late α-Capricornids at that time, a shower last clearly detected on August 17.

Figure 2 shows all meteor radiants in that part of the sky between 2020 August 16 and October 3. The top left panel shows the full period, while the subsequent panels show results for each week during that time period. The shower stands out best from the sporadic

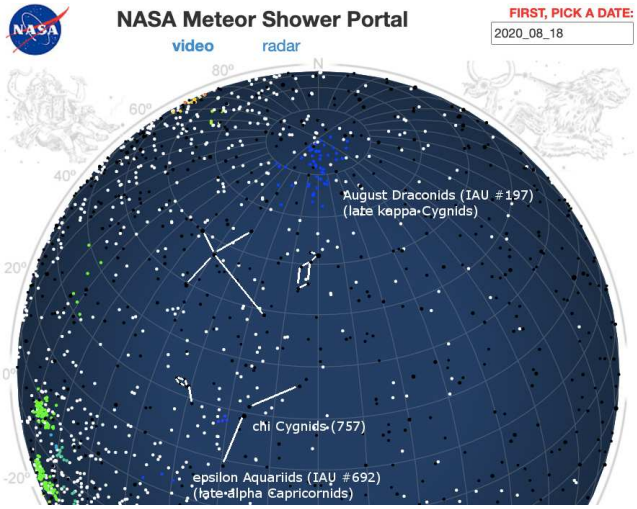

Figure 1 – Early detection of the χ-Cygnids on 2020 August 18. At this time, the radiant is in Aquila, not in Cygnus.

[1]SETI Institute, 189 Bernardo Ave, Mountain View, CA 94043, USA. Email: `pjenniskens@seti.org`

IMO bibcode WGN-485-jenniskens-ccy
NASA-ADS bibcode 2020JIMO...48..146J

Table 1 – Number of χ-Cygnids captured by each CAMS network.

Network	Cameras	Name	Operator	χ-Cygnids
1	77	CAMS California	Peter Jenniskens	15
2	27	CAMS Florida	Andy Howell	13
3	76	CAMS BeNeLux	Carl Johannink	157
5	48	CAMS New Zealand	Jack Baggaley	10
6	64	LO-CAMS	Nick Moskovitz	31
7	48	UACN	Mohammad Odeh	27
8	16	CAMS South Africa	Tim Cooper	22
10	8	CAMS Northern California	Tim Beck	2
14	40	CAMS Arkansas	Luke Juneau	16
15	48	CAMS Australia	Martin Towner	36
16	48	CAMS Chile	Steve Heathcote / E. Jehin	35
17	48	CAMS Namibia	Tony Hanke	85

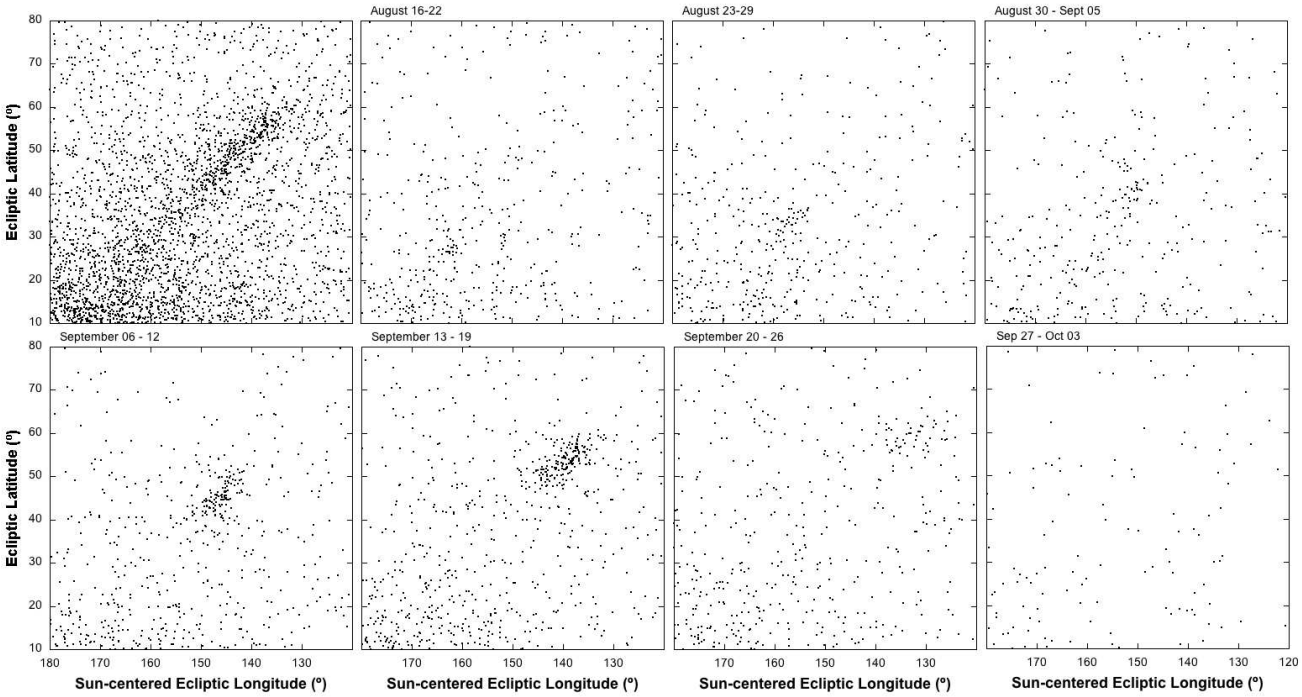

Figure 2 – CAMS-detected χ-Cygnids over the period 2020 August 16 to October 3. The top left diagram shows all data combined, while subsequent plots show meteors detected in each week during this time interval.

background in these short time intervals. The clusters were extracted as they appear in these diagrams, then velocity outliers are removed (either sporadic meteors or meteors for which the speed was calculated incorrectly). The result was that a total of 449 meteors were identified as possible stream members.

There is a hint in the data that the radiant is active earlier in time than August 18, perhaps as early as August 5 (solar longitude 133°). At that time, the radiant is close to the antihelion source and the sporadic background is strong. Hence, some of these possible stream members may be interlopers.

Figure 3 shows the number of detected meteors in each solar longitude interval. Rates increase gradually until a maximum in the week of September 13-19. After September 25, the activity comes abruptly to a halt. Figure 2 shows no hint of a shower in the week of September 27 to October 03.

Figure 4 shows the orbital elements as a function of solar longitude. The perihelion distance is gradually increasing from about $q = 0.77$ AU to $q = 0.98$ AU over the activity range, seemingly until a point where the orbits are no longer intersecting with Earth's orbit. At the same time, the inclination of the orbits is increasing from 12° to 21°. In contrast, the semi-major axis remains constant at a median value of ≈ 2.90 AU, as does the longitude of perihelion at $\approx 21\overset{\circ}{.}9$.

No single set of orbital elements completely describes the stream. A lookup table is required to capture the change in orbital elements of this warped stream over time. Table 2 gives some representative values at different solar longitude intervals.

4 Discussion

The constant longitude of perihelion and gradually changing orbital elements point to a relatively recent

Table 2 – Representative values of the stream at different solar longitude intervals.
* – As reported in Jenniskens et al. (2020); ** – From Jenniskens et al. (2015).

Year	N	Sol.Long. [°]	R.A. [°]	Dec. [°]	Vg km/s	a [AU]	q [AU]	i [°]	ω [°]	Ω [°]
2020	21	138.0	300.5	+4.0	18.1	2.75	0.784	12.4	242.3	138.0
2020	38	145.3	303.9	+7.6	17.2	2.84	0.827	12.8	236.0	145.3
2020*	8	148.0	304.7	+8.5	17.0	2.95	0.830	12.7	235.3	148.0
2020	50	154.1	304.7	+15.4	16.5	3.09	0.872	14.4	227.8	154.1
2020	49	163.6	304.0	+22.8	15.1	2.80	0.916	15.7	219.2	163.6
2020	74	167.7	302.7	+26.8	15.2	2.93	0.935	17.0	214.4	167.7
2015**	9	171.6	301.0	+32.6	15.1	2.75	0.949	18.6	209.9	171.6
2020	118	172.3	301.1	+32.5	15.2	2.90	0.951	18.4	209.8	172.3
2020	86	176.9	298.1	+37.6	15.4	2.92	0.968	19.8	204.7	176.9
2020	13	180.0	296.2	+39.9	14.9	2.89	0.976	19.6	202.2	180.0
2020 RF	(JPL)	175.6	296.9	+36.2	14.1	2.60	1.009	18.3	204.5	175.6

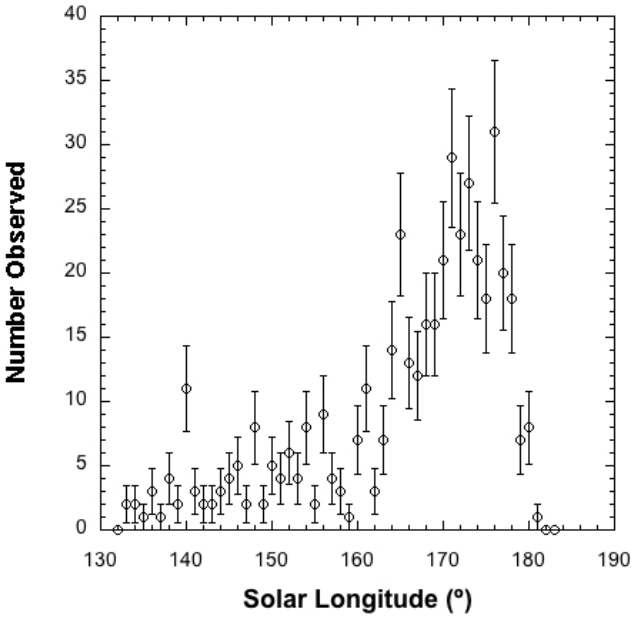

Figure 3 – Activity curve: number of detected χ-Cygnids per solar longitude interval.

fragmentation of a parent body. The orbit is fairly short and appears to be uncoupled from Jupiter (Figure 5). That points to a relatively old Jupiter-family comet or a primitive asteroid as the source. Meteors of +2 magnitude penetrate to about 82.6 km altitude. That puts them near the top of the range of penetration depths, suggesting the meteoroids are fragile, cometary in nature. Likely, we are looking for a Jupiter Family comet that was captured a long time ago. An object similar to 169P/Neat, parent of the alpha Capricornids, but that comet has a significantly different longitude of perihelion (169P: 34.°2).

Because the breakup that created the stream was relatively recent, a parent object may still be found in the stream. Specifically, we are looking for an orbit with longitude of perihelion $\approx$ 21.°9 and semi-major axis $\approx$ 2.9 AU. Searching the asteroid and comet databases for objects with inclination in the range 10°–20°, node in the range 100°–200°, perihelion distance in the range 0.5–1.2 AU, and semi-major axis in the range 2.5–3.5 AU, only provides one reasonable candidate, asteroid 2020 RF (Table 2).

2020 RF has orbital elements that more or less follow the trend seen in the meteoroid observations. The semi-major axis is relatively low at $a = 2.60$ AU and the longitude of perihelion is 20.°1. The asteroid passes close to Earth's orbit, with the last close approach to Earth of only 0.052 AU on 2020 September 17 at 02:30 TDB (cneos website). The asteroid has a Tisserand parameter of $T_J = 3.063$, which puts it just above the Jupiter-Family comet regime among asteroids. The object's absolute magnitude is only $H = 22.3$ magnitude, making it a small comet or primitive asteroid at best (for an albedo of 0.04) of only 0.23 km diameter. This object could be a mere interloper, ejected by the 2:5 mean-motion resonance of Jupiter.

Integration of the orbit is required to test if the asteroid might be related to the stream, which is beyond the scope of this report. As it stands, it is quite possible that the parent body of the χ-Cygnids has yet to be discovered.

Acknowledgements

Congratulations to the observers hosting one of the CAMS stations and to the network operators for gathering the data described in this paper. Many thanks to Pete Gural, Dave Samuels and Steve Rau for keeping the network in good shape. This work was supported by NASA grant 80NSSC19K0563.

References

Jenniskens P. (2015). "New Chi Cygnids meteor shower". CBET 4144. IAU Central Bureau for Astronomical Telegrams. D. W. E. Green (ed.).

Jenniskens P. (2020). "Possible upcoming return of the chi Cygnids in September 2020". *eMeteorNews*, **5**, 287–289.

Jenniskens P., Hanke T., Heathcote S., Jehin E., Towner M., and Cooper T. (2020). "Chi Cygnid meteor shower 2020". CBET 4837. IAU Central Bu-

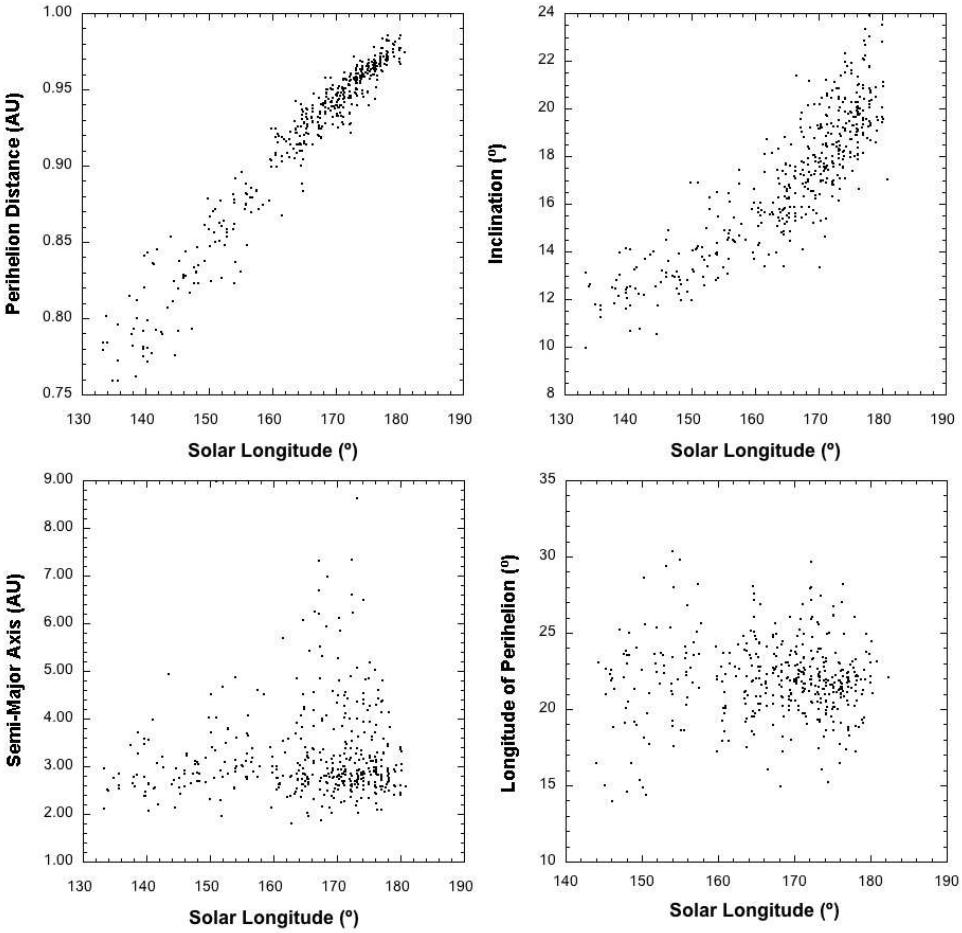

Figure 4 – Orbital elements of χ-Cygnids as a function of solar longitude (date of appearance).

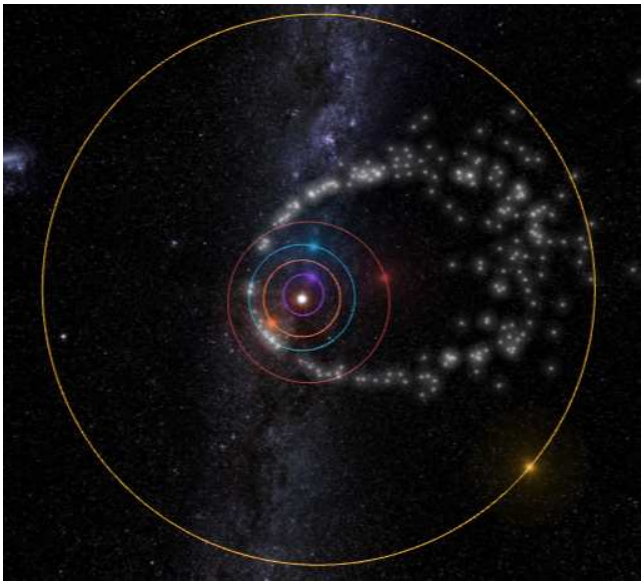

Figure 5 – Diagram of 2015 χ-Cygnid orbits. The outer circle is the orbit of Jupiter.

reau for Astronomical Telegrams. D. W. E. Green (ed.).

Jenniskens P. and Nénon Q. (2016). "CAMS verification of single-linked high-threshold D-criterion detected meteor showers". *Icarus*, **266**, 371–383.

Kornos L., Matlovic P., Rudawska R., Toth J., Hajdukova M., Koukal J., and R. P. (2014). "Confirmation and characterization of IAU temporary meteor showers in EDMOND database". In Jopek T. J., Rietmeijer F. J. M., Watanabe J., and Williams I. P., editors, *Meteoroids 2013. Proceedings of the Astronomical Conference held at A. M. University, Poznan, Poland, Aug. 26-30, 2013*. A. M. University Press, pages 225–233.

Koukal J., Srba J., and Toth J. (2016). "Confirmation of the chi Cygnids (CCY, IAU#757)". *WGN, Journal of the IMO*, **44:1**, 5–9.

Roggemans P., Johannink C., and Breukers M. (2016). "Status of the CAMS-BeNeLux network". In Roggemans A. and Roggemans P., editors, *Proceedings of the International Meteor Conference, Egmond, the Netherlands, 2-5 June 2016*. IMO, pages 254–260.

Rudawska R. and Jenniskens P. (2014). "New meteor showers identified in the CAMS and SonotaCo meteoroid orbit surveys". In Jopek T. J., Rietmeijer F. J. M., Watanabe J., and Williams I. P., editors, *Meteoroids 2013. Proceedings of the Astronomical Conference held at A. M. University, Poznan, Poland, Aug. 26-30, 2013*. A. M. University Press, pages 217–224.

Handling Editor: Jürgen Rendtel

Noctilucent Clouds over Munich in July 2020

Peter C. Slansky[1]

In July 2020 bright and colourful noctilucent clouds (NLC) could be observed from the very centre of Munich, Germany. Located at about 48° North, Munich is comparably south for NLC. During two nights the author could take some series of photos with wide angle and telephoto lenses and a video. First results of the observations were presented by the author at the online IMC 2020. A time-lapse video, which is repeatedly referred to in this article, was posted on the IMO website.[a] This article presents more detailed results of the geometrical and temporal analysis of these observations. The following goals could be achieved: 1. geographical localization of all observed NLC; 2. analysis of exemplary absolute structure sizes within selected NLC structures; 3. determination of direction and velocity of motion of a specific NLC structure, both transversal and tangential.

Received 2020 October 3

This work has been presented at the International Meteor Conference 2020 (held online).

1 Introduction

Noctilucent clouds are interesting for meteor observers because they have two important things in common with meteors: They have a cosmic origin, from which a terrestrial light effect results. And they are beautiful.

NLC occur in the mesopause, a thin layer of the Earth's atmosphere at 85 to 80 km altitude[b] between the lower mesosphere and the higher thermosphere. Due to the low atmospheric density and the thinness of the mesopause of only 5 km, NLC are very faint and transparent. So, in the visible light their observation is only possible in a certain backlight situation that is given during summer nights in northern direction (on the northern hemisphere), when with the Sun is about −8° to −16° below the horizon but still shining on the clouds. It is often claimed that their appearance is limited to the area between ±50° to 70° latitude.[a] But Munich is at about 48° North. Here the best conditions for NLC were in June/July around 3 hours before and 3 hours after astronomical midnight, with theoretical maxima at 22^h00^m CEST and 04^h00^m CEST ($20^h00^m/02^h00^m$ UT). Of course the sky must be clear of tropospheric clouds as well. All these conditions came together in Munich in some nights in early July 2020 in the most exciting way.

There is another interesting thing about NLC for meteor observers: Right in the mesopause, at the altitude of 85 to 80 km, many meteors reach their maximum brightness and glow up. Two prominent examples of this are the Perseid fireballs 3414-2018, observed by the author (Slansky & Gaehrken, 2019), and EN120812, observed by Spurný et al. (2014). In the mesopause the atmosphere has its temperature minimum. Here the dust of former meteors serves as condensation nuclei for water ice, which forms the NLC. Temperatures in the mesopause are particularly low in summer (!), which is why NLC occur almost exclusively in the summer months.

Table 1 – Air density in the high atmosphere, expressed by the number of molecules per cube meter, relative to altitude, according to Michelberger and Wurzel (2005).

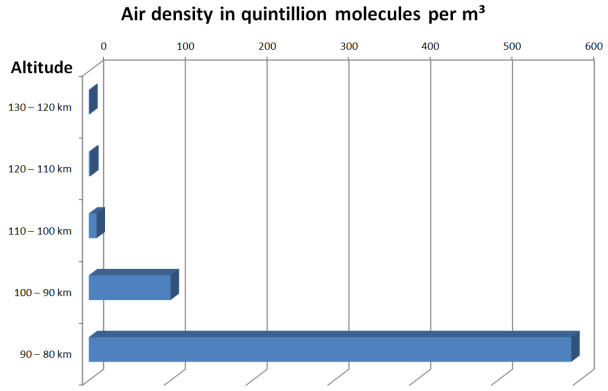

Table 1 shows that the mesopause is also characterized by a rapid increase in air density compared to the higher layers of the atmosphere. Therefore, the moment a meteor enters the mesopause, it is slowed down significantly and it lights up.

Jean-Louis Rault commented on my presentation at the online IMC 2020 that the dynamics of NLC in general are significantly influenced by gravity waves in the atmosphere. In 2017, he had participated in a multisensor observation campaign for meteors at the Observatoire de Haute-Provence, in collaboration with the Office national d'études et de recherches aérospatiales ONERA. In this campaign, two near-infrared cameras recorded gravity waves in different directions and in time-lapse – as a side effect to the intended meteor detection.[c] (These gravity waves are a purely aerodynamic phenomenon and may not be confused with gravitational waves, such as those generated when two black holes merge!) For the investigation of these atmospheric gravity waves the observation of NLC, in particular their movement and change over time, provides an excellent means (Dalin et al., 2015).

[1]Email: slansky@mnet-online.de

IMO bibcode WGN-485-slansky-nlc
NASA-ADS bibcode 2020JIMO...48..150S

[a]IMO/Slansky, Peter C.: https://www.imo.net/members/imo_video/view?video_id=150

[b]These are average numbers for summer; in winter the mesopause has a higher altitude of about 100 km: https://de.wikipedia.org/wiki/Mesosphaere.

[c]Personal information by Jean-Louis Rault.

Figure 1 – NLC over the Munich city centre on 2020 July 5, 22^h30^m CEST (20^h30^m UT). The camera was a Canon EOS 20Da at ISO 200, $t = 6$ s, with a Sigma 3.5/10-20 mm zoom lens at $f = 13$ mm and $F = 5.6$ with a field of view of $82° \times 60°$. The camera was pointed north-north-west. As can be seen the NLC exceeded the horizontal field of view.

The International Cloud Atlas[d] lists up four main types of NLC structures:

- Type I Veils: These are very tenuous, lack well-defined structure and are often present as a background to other forms ... Veils are the simplest form of noctilucent clouds and often precede ... the appearance of noctilucent clouds with well-defined structure.
- Type II Bands: These are long streaks, often occurring in groups arranged roughly parallel to each other or interwoven at small angles, but occasionally an isolated band is observed.
- Type III Billows: These are arrangements of closely spaced, roughly parallel short streaks. The distance separating adjacent billows ranges from about 1 km to 10 km ... The billows may change their form and arrangement, or appear and disappear within several minutes, much more rapidly and frequently than the long bands.
- Type IV Whirls: These are partial or, on rare occasions, complete rings of clouds with dark centres. They are sometimes seen in veil, band and billow forms.

During the nights from 2020 July 5/6 and 7/8, the author was able to observe, photograph and film all these four types of structures inside one NLC display over Munich.

2 Observation

The first NLC (of my life) I saw on 2020 July 5 at 22^h35^m CEST (20^h35^m UT) from my roof terrace in the Munich city centre. This was approximately 3 hours before astronomical midnight. The sun was $-8°$ below the horizon at an azimuth of 322°. Accordingly, the midpoint of the NLC appeared in the north-north-west. These NLC were so bright that they clearly surpassed the – truly not dark – Munich city lighting, even the illumination of the Munich Cathedral that is located 1 km from my terrace to the North. I pointed my camera at the brightness centre which was at the midpoint of the NLC. Although I used a wide angle lens giving a field of view of $82° \times 60°$ the NLCs did not fit into this field of view horizontally.

I made a first series of photos, but without time-lapse setup. Then tropospheric clouds came up. Fortunately, however, the favourable conditions repeated themselves just two nights later.

2.1 Sequence No. 1

The main observations were made during the night of 2020 July 7/8. At 22^h34^m CEST I started the first timer photo sequence. The NLC in the north-west occurred relatively close to the horizon, so they were quite far away. Veils structures were predominant. I used my Sony α7S with a Canon FD 4.0/200 mm telephoto lens, giving a field of view of $10\,^\circ\!.1 \times 6\,^\circ\!.7$ at an aspect ratio of 3:2. The camera was set to ISO 800, $t = 1/2$ s and $F = 5.6$. These NLC before midnight were already in their decline, so the exposure of this photo series ran short.

2.2 (Video-) Sequence No. 2

After midnight the conditions improved considerably and at 03^h30^m CEST the brightest and most beautiful NLC appeared. This clearly shows how crucial the light perspective of the NLC is for their apparent brightness: The shape and density of the clouds had probably not changed significantly since the time before midnight, but the light perspective definitely had. I equipped my Sony α7S with a Sony GM 1.4/24 mm wide angle lens. The camera was set to video mode at ISO 3200 and 25 fps, but with an integration time of 1/4 s at $F = 2.8$. The resulting field of view was $73° \times 45°$ at an aspect ratio 16:9. Starting at 03^h50^m CEST (01^h50^m UT) 13 minutes of video were recorded. The easier handling of the camera, without the need of a timer and of hundreds of single frame exposures, came at the price of a lower resolution of only 1920×1080 pixels (Full HD) instead of 4240×2832 pixels native resolution and a quantization of only 8 Bit. For the analysis, the video was accelerated in postproduction by a factor of 15 and individual still images were extracted.

Figure 3 is a single frame from this video sequence. All four known NLC structures – Type I Veils, Type II Bands, Type III Billows and Type IV Whirls – can be identified. Their respective development over time can be analyzed in detail in the time-lapse video.

2.3 Sequence No. 3

To examine finer structures of the NLC, for sequence No. 3 the camera set to photo mode and was equipped with a Canon FD 4.0/200 mm telephoto lens. At ISO 800 and $F = 5.6$ the exposure time was 0.8 s. At the native aspect ratio of 3:2 the field of view was $10\,^\circ\!.1 \times 6\,^\circ\!.8$ as

[d]The International Cloud Atlas:
`https://cloudatlas.wmo.int/en/explanatory-remarks-noctilucent-clouds.html`

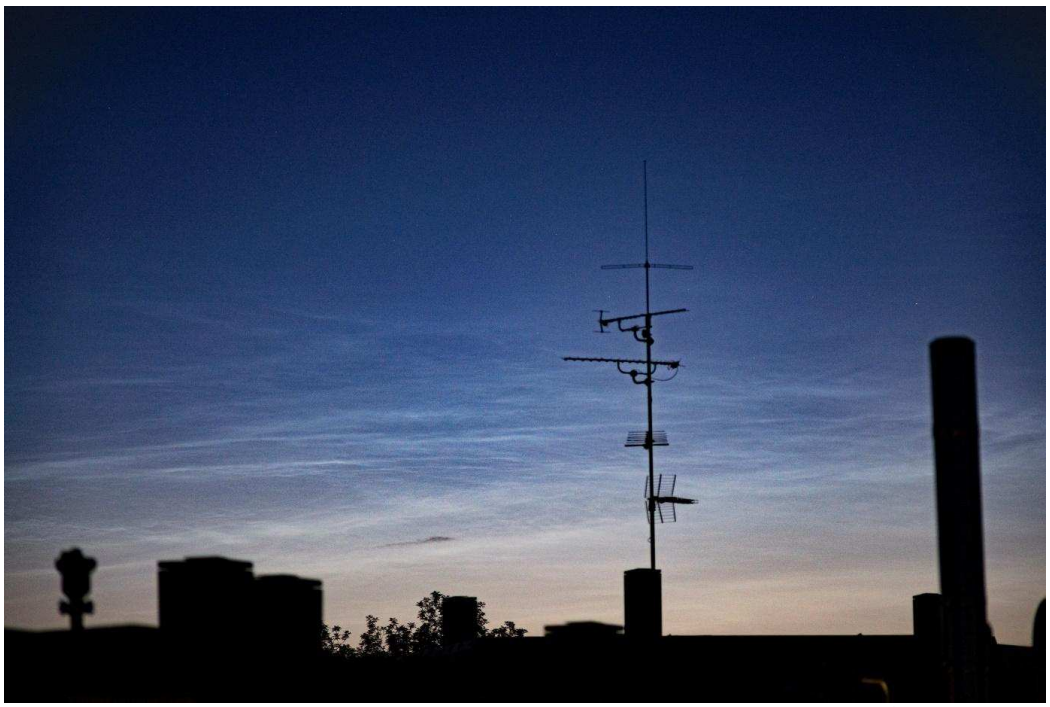

Figure 2 – This image from sequence No. 1 shows NLC over the Munich on 2020 July 7, $22^{h}40^{m}$ CEST ($20^{h}40^{m}$ UT). Camera was a Sony α7S at ISO 800, $t = 1/2$ s, with a Canon FD 4.0/200 mm telephoto lens at $F = 5.6$. These NLC in the north-west occurred relatively close to the horizon, so they were quite far away. Veils structures are predominant.

Figure 3 – Video-sequence No. 2 shows NLC over the Munich on 2020 July 8, $03^{h}50^{m}$ CEST ($01^{h}50^{m}$ UT). The image is a single frame from the original video file. The camera was a Sony α7S at ISO 3200, 25 fps and $t = 1/4$ s (!), with Sony GM 1.4/24 mm wide angle lens at $F = 2.8$, giving a field of view $73^{\circ} \times 45^{\circ}$ at 16:9. The bright star left from the image centre is Capella. The large building of the Munich town administration in the lower image centre is located in 375 m distance at an azimuth of 25° E. As will be shown later, it allowed the determination of the horizon in the image. Again, the NLC exceeded the angle of view of the camera horizontally. Note that they are much brighter than the illuminated Munich Cathedral, whose towers can be seen 1 km to the north, under the crane.

in Figure 2. Starting at $03^{h}55^{m}$ CEST 130 exposures with a timer interval of 5 s were made. In the time-lapse video, this photo series was played back 25 times faster than real time. The steps between the images were smoothened by dissolves.

Very prominent are two areas of billows structures, one with larger period in the middle left, the other one with a finer period on the upper right. Above them veils are predominant. Near the horizon dark tropospheric clouds shadow the NLC. In the time-lapse video it is striking to see how the bright NLC move east-west (right to left), while the dark tropospheric clouds in the foreground move in exactly the opposite direction.

2.4 Sequence No. 4

Besides the eye-catcher comet C/2020 F3 (NEOWISE), this sequence shows the greatest variety of different NLC structures of all telephoto image sequences. Starting at $04^{h}09^{m}$ CEST 175 exposures with an interval of 5 s were made. In the time-lapse video, this

Figure 4 – Sequence No. 3 shows the view to the horizon on 2020 July 8, $03^{h}55^{m}$ CEST ($01^{h}55^{m}$ UT). The photo was made as part of a series of 130 exposures each 5 s with a Sony α7S at ISO 800, 25 fps, $t = 0.8$ s, with a Canon FD 4.0/200 mm telephoto lens at $F = 5.6$. The original field of view is $10\overset{\circ}{.}1 \times 6\overset{\circ}{.}8$ at 3:2. Typical for near horizon NLC is the color gradient from blue to orange. Note the pronounced billows structures (NLC type III).

Figure 5 – Sequence No. 4: Comet C/2020 F3 (NEOWISE) (lower left corner) was nearly "drowning" in the NLC on 2020 July 8, $04^{h}13^{m}$ CEST ($02^{h}09^{m}$ UT). The photo was made as part of a series of 175 exposures with an interval of 5 s. The photographic parameters were the same as in Figure 4. Of all four telephoto sequences recorded, this sequence shows the richest variety of structures, in all four known types.

photo series was played back 32 times faster than real time. From the start to the end of this sequence veils, bands, billows and whirls occurred. Figure 5 was taken at $04^{h}13^{m}$ CEST. It shows veils in the lower right area, bands and billows in the middle and upper left area and whirls in the middle upper area. In this image sequence the whirls were especially impressive. They appeared more often in entire chains. Noticeable were their dark holes or "eyes", as if the NLC were punctuated at these points. Their movement was complex, especially when they moved over billows structures.

2.5 Sequence No. 5

In image sequence No. 5, isolated, faint and thin billows structures were the target. Starting at $04^{h}30^{m}$ CEST, 65 shots were taken with an interval of 5 s, then

Figure 6 – Sequence No. 5 shows faint billows-structures in the outer areas of the NLC shot on 2020 July 8, 04^h30^m CEST (02^h30^m UT). The photo was made in the beginning of a series of 65 exposures with an interval of 5 s. The photographic parameters were the same as in Figure 4. The structures moved quickly from right to left out of the field of view, so that the sequence was ended after only 5.5 minutes. Nevertheless, the time-lapse clearly reveals that every point in this NLC structure performs a roller coaster-like motion, with a transverse component from the right to the left (east-west) and a tangential component along the wave structure.

the faint billows drifted out of the field of view. But before that, their movements could be analysed in detail, and the differences in the transverse and tangential movements became apparent. In the time-lapse video, this photo series was played back 32 times faster than real time. By this, the video clearly reveals that every point in these billows structures performs a roller coaster-like motion, with a transverse component from the right to the left (east-west) and a tangential component along the wave structure.

3 Geometric-temporal analysis

For the examination of my NLC image series I set myself the following goals:

1. Geographical localisation of all observed NLC
2. Analysis of exemplary structure sizes within an NLC
3. Determination of direction and speed of movement of a certain NLC structure, both transverse and tangential.

All these goals could be achieved.

Because of their known altitude of 85 to 80 km above sea level, the approximate distance of NLC from the observation site can be calculated. For this purpose Hinz and Hinz (2015) have published Table 2.

Table 2 – Altitude of NLC related to their distance, according to Hinz and Hinz (2015).

NLC elevation above the horizon	Distance related to height above sea level
0°	1020 km
2°	820 km
4°	670 km
6°	550 km
8°	460 km
10°	400 km
15°	280 km
20°	220 km
25°	170 km
30°	140 km
45°	80 km
60°	50 km
75°	20 km

3.1 Analysis of the geometry of the NLC from Figure 3

Figures 3 and 4 were analyzed with the values from Table 2. In both images the horizon line is obstructed by buildings, but its position could be estimated in Figure 3 from the large building of the Munich city administration in the centre of the image below, which is located 375 m northeast of the observation site. On this basis the grade lines from Table 2 were plotted into the image with the corresponding distances. For simplification, the angular degrees were assumed as a linear ratio of the vertical image angle of 45° instead of a trigonometric calculation. The resulting errors are acceptable.

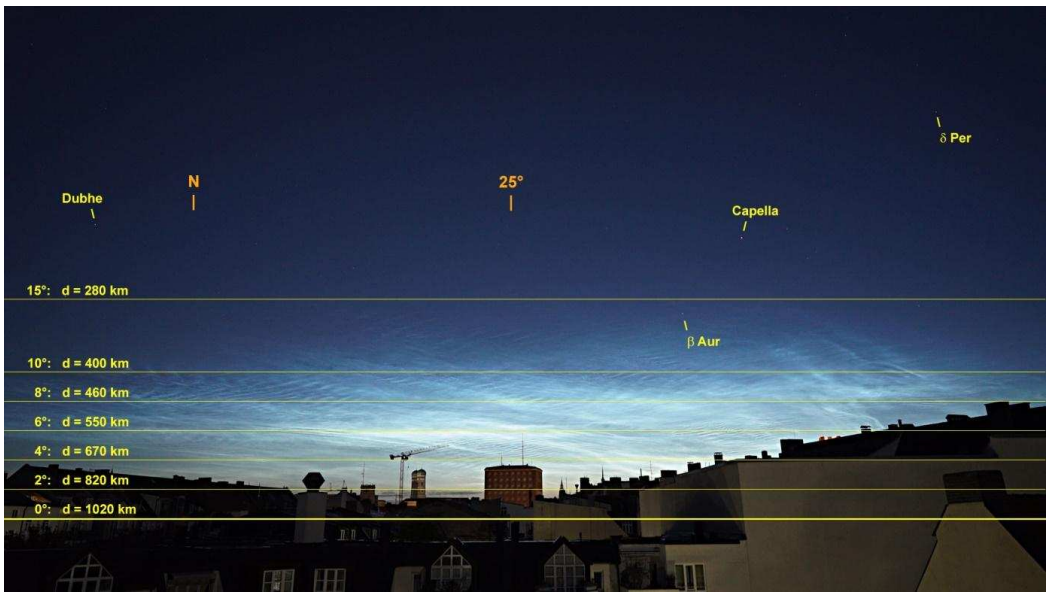

Figure 7 – Analysis of the geometry of the NLC from Figure 3. The horizon line is obstructed by buildings, but its position could be estimated from the large building of the Munich city administration in the lower centre of the image, which is located 375 m north-northeast of the observation site. On this basis the grade lines from Table 2 with the corresponding distances were plotted into the image. For simplification, the angular degrees were assumed as a linear ratio of the vertical image angle of 45° instead of a trigonometric calculation.

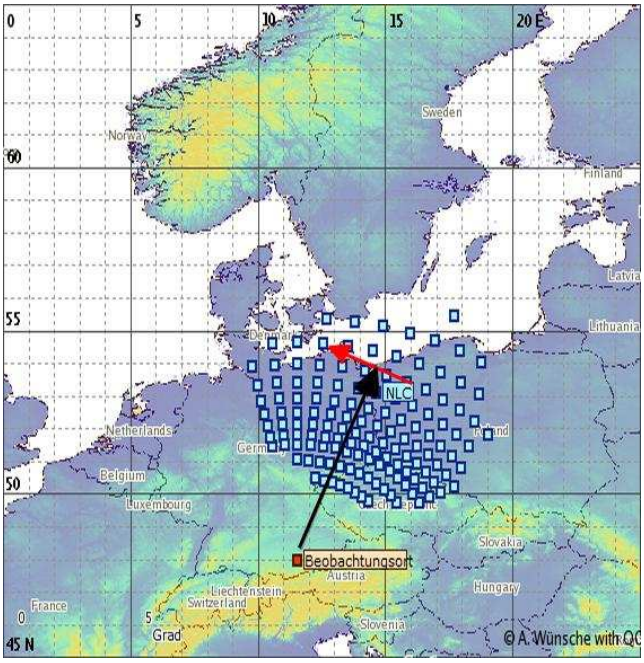

Figure 8 – Map of all NLC structures in Figures 3 and 4 (respectively Figures 7 and 9), plotted by Wuensche's website.[e] The blue squares indicate the distribution of the NLC on 2020 July 8 in Figures 3 and 4, the black arrow marks the camera alignment with the distance of the structures from Figure 4 (685 km); the red arrow indicates the direction of the transversal movement of the NLC structure from Figure 10 (see Chapter 3.4).

3.2 Map of the NLC in Figures 3 and 4

Wuensche runs a very helpful website that makes it easy to create maps of NLC.[e] All NLC positions from Figure 7 were entered in here. Figure 8 shows the result: The NLC on 2020 July 8 covered a large area over northern Czechia and north-eastern Germany to northwestern Poland up to the Baltic Sea.

The analysis of the time-lapse sequences of Figures 4, 5 and 6 reveals that the billows-structures do not just move in transversal direction but show a superposition of a transversal with a wave-shaped tangential movement. So, for a certain point in this billows structures the tangential speed is significantly higher than the transversal speed. Whirl structures show an even more complex temporal development. Finally, the image series also contained some wave structures that behaved like almost static barriers to other incoming structures in their paths.

3.3 Analysis of the size of the billows-structures in Figure 4

Starting from the intersection of the "reference billows" in the middle of the image with the 4°-line, indicating a distance of 670 km, four more billows were counted along the orange arrow. By perspective interpolation the distance of the upper point of the orange arrow from the camera was calculated to 627 km. Therefore the upper left end of the orange arrow is 43 km closer to the camera than the lower right end. Thus a triangulation for the three-dimensional perspective corrected length of the orange arrow could be performed to 49 km. Divided by the considered number of billows (four) this results in a mean billows-period of about 12 km. This is a little bit more than the maximum billows size of 10 km according to the International Cloud Atlas (see Chapter 1). As can be seen in Figure 9, too, the period of the billows in the right part of the image is only about half that size.

[e] Wuensche, Alexander:
`http://www.leuchtende-nachtwolken.info/kalkulator.htm`

Figure 9 – Analysis of the period of the billows-structures from Figure 4: Starting from the intersection of the "reference billow" with the 4°-line, indicating a distance of 670 km, four more billows were selected and counted along the orange arrow. By perspective interpolation the distance of the upper point of the orange arrow from the camera to 627 km was calculated. Therefore the upper left end of the orange arrow is 43 km closer to the camera than the lower right end. Thus a triangulation for the three-dimensional perspective corrected length of the orange arrow could be performed to 49 km. Divided by the considered number of billows (four) this results in a mean billows-period of about 12 km.

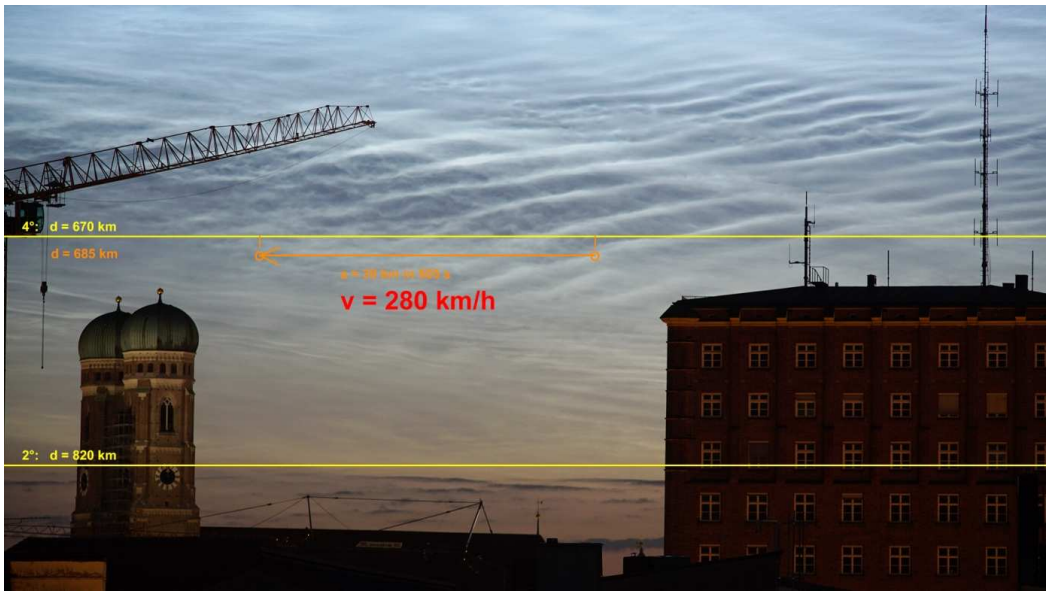

Figure 10 – Analysis of the movement of a certain point of a billows-structure from Figure 4. Although the horizon is outside the field of view in this image, the 4°-line and the 2°-line can be clearly identified by the crane cab and the dial of the tower clock. The structure in the orange circle on the right moved exactly in horizontal direction to the left. It was followed over 101 single frames (= 505 seconds) to the orange circle on the left. Because the orange arrow is a little bit below the 4°-line, that indicates a distance of 670 km, interpolation results in a distance of this structure of 685 km from the camera. Counting the pixels revealed a lateral movement of 39 km to the left within 505 seconds (101 frames), resulting in a lateral speed of 77 m/s or 280 km/h.

3.4 Analysis of the movement of the NLC in Figure 4

Although the horizon is outside the field of view, the 4°-line and the 2°-line could be clearly identified. The marked NLC structure moved exactly in horizontal direction along the orange arrow from the circle right from the centre to the circle on the left. Because the direction of the movement is a little bit below the 4°-line, interpolation results in a distance of this moving structure of 685 km from the camera. Pixel counting revealed a lateral movement of 39 km to the left within 505 seconds (101 frames), resulting in a lateral speed of 77 m/s (= 280 km/h). According to Larsen (2002), this is quite a high value.

4 Discussion

During two nights from 2020 July 5 to 8, I was able to observe, photograph and film all four main types of noctilucent cloud's structures over Munich. In the analysis of this photographic material, all the three objec-

tives set could be achieved: the geographical localisation of all observed NLC, the analysis of an exemplary structure size within an NLC and the determination of the direction and the speed of movement of a certain NLC structure, both transverse and tangential. NLC structure sizes as well as their moving velocity both were comparably high.

Compared to meteors, NLC are easy to observe – visually, by photo or by video –, if they are bright enough. Time-lapse videos allow detailed analysis of their – complex – temporal development and movement. The appearance of NLC is directly related to the residues of burnt meteors and their interaction with the mesopause: NLC are formed by water ice around meteor dust as condensation nuclei. So, they are interesting for meteor observers as well as for aeronomists. Further – joint? – observation and analysis seems to be highly valuable for both disciplines.

Based on these results and from an amateur's point of view, I would like to raise the following questions:

- NLC are a phenomenon at the intersection of two scientific disciplines, aeronomy and meteor observation. Both are local phenomena. What role could amateurs of both disciplines play in their further investigation? How could their cooperation across the disciplinary boundaries be improved?
- For the observation of NLC the special light perspective described must be given. Which are, under these conditions, the possibilities and the limits of stereoscopic multi-station photography of NLC?
- As can be seen in the wide angle images, NLCs are more bluish at higher elevations over the horizon and more orange at low elevations over the horizon. So, should it be interesting to observe NLC at higher elevations in the near ultra-violet and at lower elevations in the near infrared?
- With a thickness of only 5 km, the mesopause represents a very thin atmospheric layer. Do billows-structures of NLC lie completely within this thickness? Or does the mesopause itself show a wave-shaped formation at these positions? What role do gravity waves play in this?
- Since NLC consist of water ice crystals, they should represent a significant local increase of the atmospheric mass density. Does this have an effect on a meteoroid that enters a NLC in the mesopause? Can a NLC cause or promote an increase in brightness of a meteor or can it even cause a terminal flash?

Notwithstanding this, time-lapse photography appears to be a highly appropriate means of further investigation of NLC. It should also be observed at wavelengths other than those of visual light. The author will be happy to discuss and share his results and data with any interested scientist and to adopt ideas for future observations.

Acknowledgements

I want to thank Jean-Louis Rault, Observatoire de Paris and IMO radio commission, for his highly valuable personal information to me about the gravity waves and the link to the article of Dalin et al.

References

Dalin P., Pogoreltsev A., Pertsev N., Perminov V., Shevchuk N., Dubietis A., Zalcik M., Kulikov S., Zadorozhny A., Kudabayeva D., Solodovnik A., Salakhutdinov G., and Grigoryeva I. (2015). "Evidence of the formation of noctilucent clouds due to propagation of an isolated gravity wave caused by a tropospheric occluded front". *Geophysical Research Letter*, **42:6**, 2037–2046. 10.1002/2014GL062776.

Hinz C. and Hinz W. (2015). "Lichtphaenomene | Farbspiele am Himmel". *Oculum*, page 192.

Larsen M. F. (2002). "Winds and shears in the mesosphere and lower thermosphere: Results from four decades of chemical release wind measurements". *Journal of Geophysical Research*, **107:A8**, 1215. 10.1029/2001JA000218.

Michelberger J. and Wurzel R. (2005). "Earthgrazer – Wunder des Himmels". *Sterne und Weltraum*, **11**, 76–83.

Slansky P. C. and Gaehrken B. (2019). "3414-2018: A Perseid fireball showing exceptional light effects, observed by video, photo and radio". *WGN, the Journal of the IMO*, **47:3**, 79–92.

Spurný P., Shrbený L., Borovička J., Koten P., Vojáček V., and Štork R. (2014). "Bright Perseid fireball with exceptional beginning height of 170 km observed by different techniques". *Astronomy & Astrophysics*, **563**, A64.

Handling Editors: Jean-Louis Rault and Javor Kac

Enhanced activity of the Aurigids 2019 and predictions for 2021

Jürgen Rendtel[1], *Esko Lyytinen*[2], *Jerèmie Vaubaillon*[3]

The Aurigid meteor shower is known since its first remarkable activity observed in 1935 by Hoffmeister and associated with comet C/1911 N1 (Kiess). An outburst was predicted and subsequently observed in 2007. Other rate enhancements have been reported in other years. In 2019, the ZHR level was significantly above the average, while the population index was very close to the long-term average value of $r = 2.50$. A peak ZHR $= 62 \pm 12$ is found at $\lambda_\odot = 157\,^\circ\!.918$ (2019 August 31, $21^\mathrm{h}22^\mathrm{m}$ UT) which is close to the node at $\lambda_\odot = 158°$. A possible explanation for this activity is the existence of a very elongated 1-revolution trail released from the parent an orbit earlier than 1935. Enhanced rates are expected to occur during the 2021 return close to $\lambda_\odot = 158\,^\circ\!.396$ on 2021 August 31, $21^\mathrm{h}35^\mathrm{m}$ UT.

Received 2020 September 6

This work has been presented at the International Meteor Conference 2020 (held online).

1 Introduction

Meteors of the Aurigids (sometimes called α-Aurigids) were first reported in the morning of 1935 September 1 when Teichgraeber and Hoffmeister in Sonneberg (Hoffmeister, 1936) as well as Vrátnik, Vlček and Štěpánek in Prague (Guth, 1936) observed noticeable meteor activity from a radiant at $\alpha = 86°$, $\delta = 40\,^\circ\!.5$ (1925.0). Rates corrected only for the radiant elevation (no limiting magnitudes given) yielded 26 in Germany and 29 for the Prague team. Assuming that the limiting magnitudes were below the reference value of 6.5 mag, the actual ZHR might have been higher by a factor of 2. There are no indications of an earlier appearance of meteors from this radiant (Rendtel, 1990).

Guth (1936) found a quite close coincidence between the parabolic elements of the meteoroid stream and Comet C/1911 N1 (Kiess). This comet has an orbital period of about 2500 years (semi-major axis $a = 184$ AU), but the meteoroid orbits are considerably smaller than the parent's orbit. In the period 1988–2000, the annual Aurigid activity reached a ZHR of 7 ± 1 at $\lambda_\odot = 158\,^\circ\!.6 \pm 0\,^\circ\!.01$ and an average $r = 2.6 \pm 0.1$ with a slight minimum around the time of maximum activity (Dubietis & Arlt, 2002). More recent rate data from 2007 to 2019 are listed in Table 1.

Outbursts of short duration have been reported in 1935, 1986, 1994 (Jenniskens, 2006), and 2007. The 2007 outburst was predicted by Lyytinen and Jenniskens (2003) with an update by Jenniskens and Vaubaillon (2007) and details about the modelling are given in (Jenniskens and Vaubaillon, 2008).

Since the Aurigids follow the most attractive Perseids only by about two weeks, the attention to observe this minor shower is limited and the data coverage is not complete in most years.

Already while checking the incoming data to the IMO's VMDB a generally high ZHR in 2019 was obvious. This sometimes happens if there are (many) intervals with a low radiant position. However, this was not the case in 2019 and enforced a detailed look into the shower's return.

Optical observations of the 2020 Aurigid return were affected by bright moonlight. The (currently stored) visual data hint at a ZHR of about 5–10 and preliminary video data give a flux density below $2\,/(1000\,\mathrm{km}^2\,\mathrm{h})$ which are close to the "usual" maximum values.

2 Data of the 2019 return

For this study we collected visual, video and radio forward scatter data reported by observers worldwide. The graphs shown here consider data available by 2020 June 12 (visual, video).

Visual data for entire activity profile have been submitted to the IMO's VMDB by 16 observers (sessions/hours effective time/Aurigids): Pierre Bader (9, 17.4, 33), Christoph Gerber (3, 2.4, 2), Jiri Konečny (1, 2.1, 18), Hynek Krejzlik (1, 2.1, 14), Lukas Krejzlik (1, 2.1, 17), Katerina Krumpholcova (1, 2.1, 18), Koen Miskotte (2, 4.1, 5), Štěpán Ptáčník (1, 2.1, 19), Ina Rendtel (6, 11.1, 38), Jürgen Rendtel (10, 31.8, 186), Terrence Ross (10, 13.6, 33), Stefan Schmeissner (3, 6.9, 5), Ivan Sergey (4, 3.9, 6), Roland Winkler (2, 2.8, 4), Anna Wrnatova (1, 2.1, 14), Oliver Wusk (3, 7.0, 11).

The resulting general ZHR profile for the entire Aurigid return from end August to early September 2019 is shown in Figure 1. While the typical maximum ZHR level for most returns is of the order of 10 (see Table 1), the 2019 values were significantly higher. We find a ZHR ≈ 10 for most of the activity period, and higher values in the maximum night.

For the **video data** analysis we used the temporary data base which is accessible via the meteorflux webpage `https://meteorflux.org/` (access date as indicated in the Figure caption). Throughout the paper we shorten flux density into flux.

[1]Leibniz-Institut für Astrophysik, An der Sternwarte 16, 14480 Potsdam, Germany
and International Meteor Organization, Eschenweg 16, 14476 Potsdam, Germany.
Email: `jrendtel@web.de`
[2]Ursa, Finnish Fireball Network, Kehäkukantie 3 B, 00720 Helsinki, Finland.
Email: `esko.lyytinen@jippii.fi`
[3]IMCCE, Observatoire de Paris, PSL Research University, CNRS, Sorbonne Universités, UPMC Univ. Paris 06, Univ. Lille, France.
Email: `Jeremie.Vaubaillon@obspm.fr`

IMO bibcode WGN-485-rendtel-aur
NASA-ADS bibcode 2020JIMO...48..158R

Radio forward scatter data do not show any increase (H. Sugimoto, personal communication on 2020 March 14).

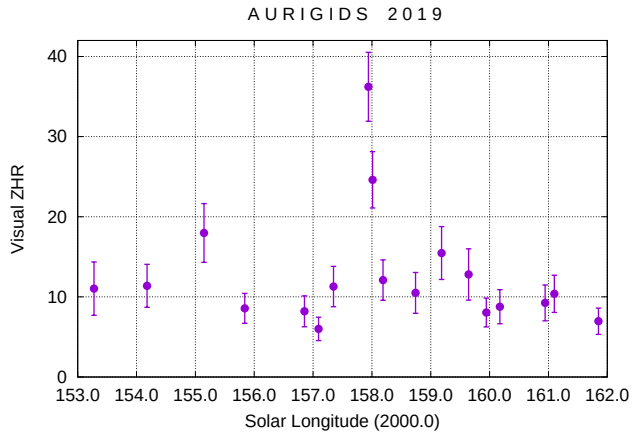

Figure 1 – Visual Aurigid ZHR of the 2019 return between August 27 ($\lambda_\odot = 153°$) and September 5 (162°). We applied a population index $r = 2.50$ for the entire period (see discussion in section 3). The minimum binning interval length was set to 3 hours, the minimum AUR number per interval is 15.

Table 1 – **Aurigid maximum data** in the period 2007 – 2019 derived from visual data. Since we look for the general peak level, we used a bin width of 1–2 hours (depending on the amount of data in the respective year) and a constant $r = 2.50$, except for 2007 where $r = 1.74$. (The "day" refers to Aug 31 or Sep 01; Int, AUR – number of intervals and Aurigid meteors defining the peak value.)

Year	Day	UT	$\lambda_\odot$	Int	AUR	ZHR
2019	31	22:25	157.96	20	106	32±3
2018		no maximum data				
2017	31	18:08	158.29	5	13	8.2±2.2
2016	01	02:13	158.85	6	16	6.5±1.6
2015		no maximum data				
2014	01	09:53	158.70	3	9	7.4±2.3
2013	01	01:32	158.60	5	11	18±5
2012		no maximum data				
2011	01	18:43	158.82	3	8	10±3
2010	01	03:17	158.45	6	9	9±3
2009	31	21:55	158.49	11	15	7.3±1.8
2008	31	01:29	157.91	11	46	11±2
2007	01	11:21	158.56	22	130	150±13

3 The 2019 Aurigid peak

The listed population index of the Aurigids is $r = 2.50$. We checked the available magnitude data and calculated r for the 2019 return as this may be useful for later discussion of the meteoroid stream. For comparison we also determined an average r based on data of the period 1998–2018, excluding the 2007 outburst data. This event was characterized by a large fraction of bright Aurigids and which yielded $r = 1.74 \pm 0.08$ (Rendtel, 2007). The available profiles and the 2007 value are shown in Figure 2. It is obvious that all r-values of the 2019 return completely agreed with the average profile, and the reference value $r = 2.50$ is a very good representation of the meteor brightness distribution. The profile might suggest there is a slightly lower $r = 2.30 \pm 0.18$ near $\lambda_\odot = 157.^\circ8$ in both the average and the 2019 profiles. However, the variation is just of the order of the error margins and may therefore be no significant effect.

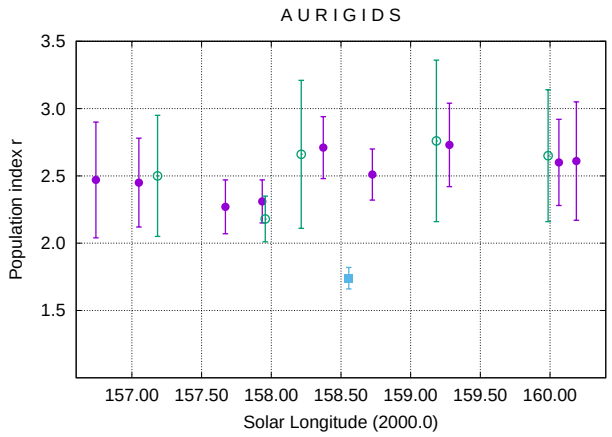

Figure 2 – Population index r of the Aurigids 2019 (circles) and the average profile from the period 1998–2018 (dots), excluding 2007. The 2007 value (square) is added for comparison.

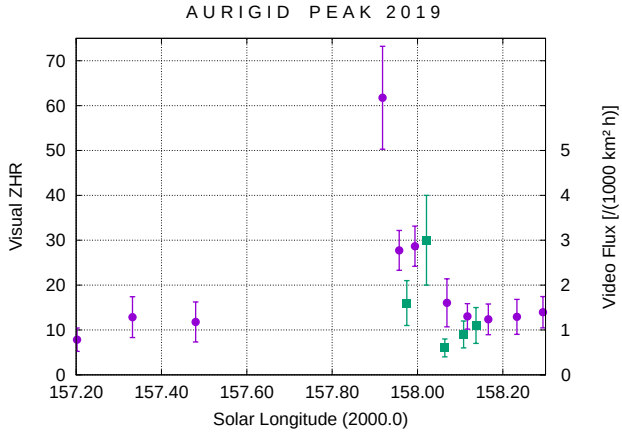

Figure 3 – Aurigid activity of the 2019 peak night. The magnitude data are not different from the nights before and after the peak, we also applied a population index $r = 2.50$ for this period. The visual ZHRs (dots) are calculated for a minimum bin length 30 minutes, minimum AUR meteors per bin 25. The video flux density (squares) is determined from the temporary database of the IMO VMO (accessed 2020 June 6).

Both, the visual and video data show a brief rate or flux enhancement in the night August 31/September 1 as shown in Figure 3. In the case of the video flux this mini peak is built of only one value. The visual data yield a slightly wider peak with no data of the ascent and possibly the peak itself. The highest ZHR = 62±12 is found at $\lambda_\odot = 157.^\circ918$, corresponding to 2019 August 31, 21^h22^m UT. It is based on five intervals and contains only 28 Aurigid meteors. However, the subsequent data points, all based on a comparable sample, strongly indicate that we indeed see a descent from a maximum with rates reaching the "typical ZHR level" between 01^h and 02^h UT. This all happens in the night

hours for European observers with a radiant elevation continuously increasing and no change in other parameters happening in this period causing inconsistencies.

This is a strong hint at enhanced activity from the stream lasting for a short time. The duration cannot be derived from the visual data because there are no values defining the ascent.

4 Model calculations

4.1 The 2019 Aurigids

There were no predictions of any density enhancement known for the 2019 return of the shower. We find the 1-revolution trail of the parent comet C/1911 N1 to pass 2019 in a (radial) distance of the nodes of about −0.0045 AU (Figure 4). Due to the geometry of the parent and Earth's orbit, this corresponds to a minimum distance of to the meteoroids of 0.003 AU. This is probably too far for observable activity and, additionally, the solar longitude of the closest approach (158 °.603) differs by almost 0 °.7 from the observed position. Hence we need to look for an other explanation. Generally, trails of more than 1-revolution may cause outbursts of some level for showers like the Lyrids (orbital period less than 500 years), but this is not expected for this long period case.

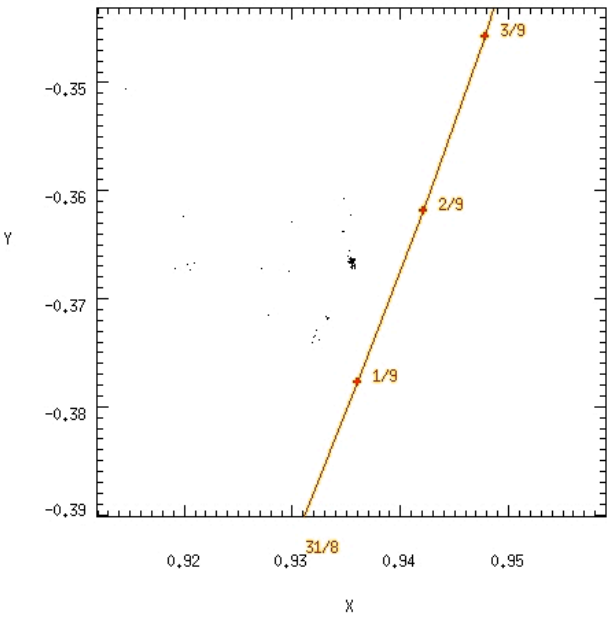

Figure 4 – Approach of the Earth to the 1-revolution trail of Aurigid meteoroids ejected in 1911 during the return in 2019 (if it would contain meteoroids). This indicates that the 2019 activity is probably not caused by the "fresh" 1-revolution trail (model of J.V., see Jenniskens and Vaubaillon, 2008) but may be material from an extended older 1-revolution trail.

4.2 Possible explanations

One possible explanation is that there may be another parent comet near the orbit of C/1911 N1. A candidate may be C/1790 A1 (Herschel) which was observed for only about 12 days. Actually it is not possible to say whether it is on the same orbit or not.

Another suggestion may be more likely. Under some circumstances, the 1-revolution trail length (expressed in years) is proportional to the power 2.5 of the semimajor axis (or to the power 5/3 of the orbital period). The effect acts in a way that it extends the trail even more for long periods. Hence it lengthens a trail quite rapidly with the orbital period and actually much faster. Such a dust trail dynamics has been described for another long-period case by Jenniskens, Lyytinen and Baggaley (2020). The stretching also strongly dilutes the trail. In principle the trail length (in years) can get longer than two times the orbital period which might be possible here.

This would mean that, while the normal 1-revolution trail would have ejected in the return prior to the 1911 return, in this case (*if* this is the correct explanation) would have been ejected even one revolution earlier (i.e. more than two comet revolutions earlier from now), but still would be only a one revolution trail.

According to comparisons with the 1-revolution Leonid trail, the 1-revolution and 2-revolution trail lengths would correspond to an approach about 1.5 years after the Leonid parent, still quite favourable for the Leonids (and a lot more diluted by the stretching). In this comparison we did not take into account that the perihelion distance of the Aurigid parent C/1911 N1 is smaller (0.6838 AU) than the Leonid parent 33P/Tempel-Tuttle (0.9766 AU), which would to some degree be more favourable for the Aurigid conditions.

The course of this trail would follow quite closely the normal 1-revolution trail, only displaced from it by a practically constant value, both in miss-distance and solar longitude.

Because we do not know the actual perihelion times of the comet before 1911, we do not know where the corresponding trail would be situated. But *(again: if)* this is the correct explanation, we can use it for further prediction. However, the future predictions according to the "extended 1-revolution trail" and the "other comet fragment" would practically coincide.

But also the following might be possible – although much less probable: the parent would have earlier been in a closer orbit with a shorter orbital period and left meteoroids in a resonance orbit which would need approximately 100 years (or less) or the meteoroid periods would have shortened by a random effect and/or the Poynting-Robertson effect, until being trapped into some resonance. Assuming a period of about 100 years, it would have taken time for the comet to alter to considerably longer period and/or the meteoroids to alter into the resonance period. And even at around 100 years period resonances, we assume that the resonance would not be efficient enough.

We think the "extended diluted trail" explanation is most probable and we see a 1-revolution trail in an orbit over (a bit more than) two comet revolutions. In this case, the meteors would have been (considerably) dimmer than in the 2007 outbursts and in the expected 2021 outburst (see below), which may be the only way of telling more about the explanations. Then it would of course be possible to predict further outbursts of the

shower. But according to our lookup, the situation is quite poor for this.

Till 2071 there does not seem to be any favourable year. The most promising returns would be in 2043 and 2044, but are perhaps not good enough. As to the possibility of shorter revolution resonant orbit, this prediction is not valid and this probably can not be predicted further (unless we obtain more information of this).

Further, if the radiant in 2019 could be derived accurately, this can perhaps tell us something more (the video data analysis is still pending). In any case, *if* the 1-revolution over 2-revolutions explanation is valid, it would probably be the first time ever that such a trail was observed. Interestingly, the magnitude distribution of the 2019 encounter does not show differences to the average found from the period 1998–2018 which implies that the meteoroid size distribution resembles the average of regular returns without rate enhancements.

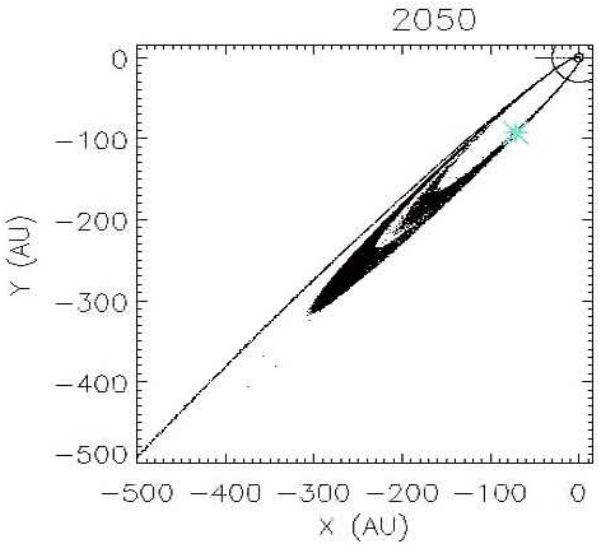

Figure 5 – Image from a simulation of a 1-revolution trail with $a = 500$ AU which hits the Earth (circle upper right edge) while the parent (asterisk) completed 2 revolutions (model of J.V.; see Jenniskens and Vaubaillon, 2008).

In Figure 5 we show the final image of a simulation of an object with a semi-major axis of $a = 500$ AU. Here the Earth encounters an extended 1-revolution trail while the parent comet has already done 2 revolutions.

We can clearly see that
– a leading trail can have completed 2 revolutions while the comet has 1 revolution;
– a trailing trail can have completed 1 revolution while the comet has 2 revolutions.

5 Expectations for the Aurigids 2021

When we checked the Aurigid conditions for the IMO Meteor Shower Calendar 2021 (Rendtel, 2020), we found that these look very favourable (Table 2). In the two existing trail-calculations (assuming slightly different orbital periods), it appears even more favourable. The miss distances in the mentioned trails are +0.0003 AU and +0.0002 AU while the new calculations give +0.00017 AU (Figure 6).

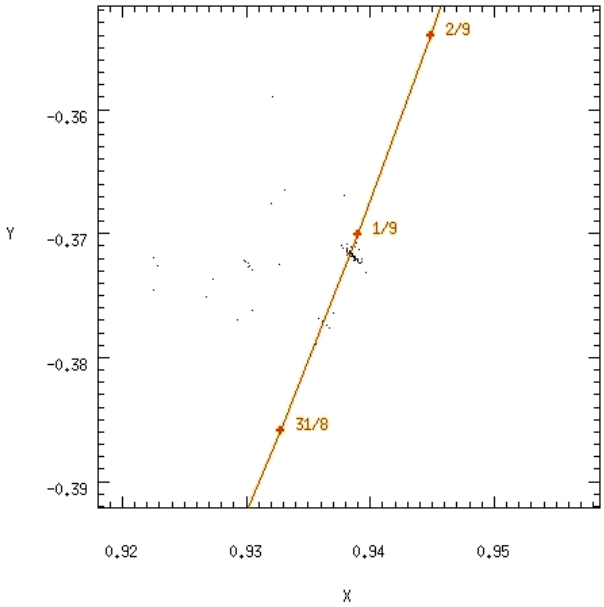

Figure 6 – Modelled approach of the Earth to the Aurigid stream in 2021.

If the encounter occurs after the perihelion (argument of perihel about 110° and encounters are in the descending node at 180°, i.e. about 70° after the perihelion. So assumed ejection near the perihelion mostly towards the Sun side would make the + sign encounters more favorable than those related to the − sign (which was the case for all previously observed cases). According to this reasoning, the 2021 Aurigids could be even better than the 2007 encounter for which the geometry is shown in Figure 7.

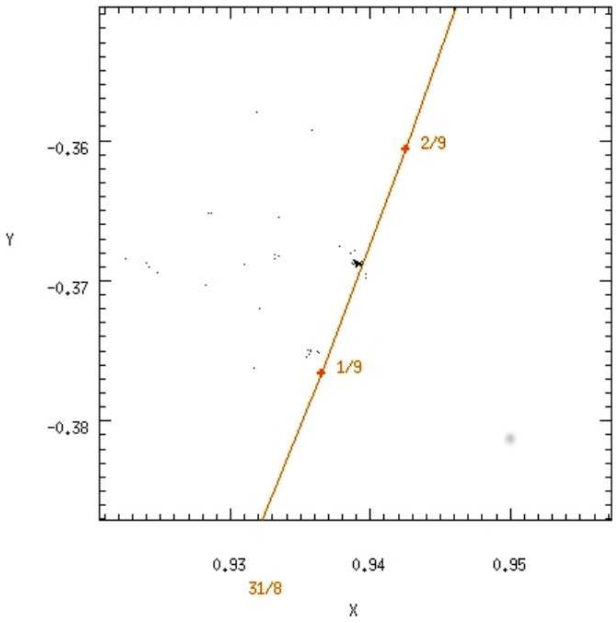

Figure 7 – Modelled approach of the Earth to the Aurigid stream in 2007 when a brief peculiar outburst of bright shower meteors was observed.

Table 2 – Results from model calculations for the Aurigid return on 2021 August 31. The values of Lyytinen and Vaubaillon are from this work; Mikiya Sato communicated his results to the authors on 2020 June 12.

Author	Min. dist.	Peak $\lambda_\odot$	2021 Aug 31
Lyytinen	0.00017 au	$158\overset{\circ}{.}395$	$21^{\rm h}35^{\rm m}$ UT
Vaubaillon	0.0001 au	$158\overset{\circ}{.}396$	$21^{\rm h}35^{\rm m}$ UT
Sato	0.00054 au	$158\overset{\circ}{.}383$	$21^{\rm h}17^{\rm m}$ UT

These predictions are quite close to each other and should allow us to test the assumptions and model parameters applying different observing techniques.

6 Conclusions

The general activity level of the Aurigids observed in 2019 exceeded the average over the past years significantly. Although the peak period is not covered completely – the ascent is not well defined – the ZHR and flux density values allow us to establish a peak at $\lambda_\odot = 157\overset{\circ}{.}918$, corresponding to 2019 August 31, $21^{\rm h}22^{\rm m}$ UT. The closest approach to an assumed Aurigid trail yields a minimum distance of 0.003 au from the Earth. This is too far away to cause an outburst and occurred about $0\overset{\circ}{.}7$ later than the observed peak. One explanation for the observed activity is the existence of a very elongated 1-revolution trail released from the parent two revolutions earlier than the 1911 return. The meteor magnitude data of the 2019 return show no deviation from the long-term average. Both yield $r = 2.50$ for the days around the maximum. An insignificantly lower value of $r = 2.30 \pm 0.18$ is found near $\lambda_\odot = 157\overset{\circ}{.}8$ in the 2019 data as well as in the average r-profile.

Enhanced rates are expected to occur in 2021. Independent model calculations are presented and hint at highest rates at $\lambda_\odot = 158\overset{\circ}{.}395$ which is on August 31, near $21^{\rm h}30^{\rm m}$ UT. The activity level is difficult to estimate as we have no information about the density in the trail and the extended length of the trail may have caused an additional dilution. Some weak indications can be interpreted in a way that the rates are relatively high.

References

Dubietis A. and Arlt R. (2002). "Annual activity of the Alpha Aurigid meteor shower as observed in 1988–2000". *WGN, Journal of the IMO*, **30**, 22–31.

Guth V. (1936). "Über den Meteorstrom des Kometen 1911 II (Kiess)". *Astron. Nachr.*, **258**, 27–30.

Hoffmeister C. (1936). "Unerwarteter Meteorstrom". *Astron. Nachr.*, **258**, 25–26.

Jenniskens P. (2006). *Meteor Showers and Their Parent Comets*. Cambridge University Press. 175ff.

Jenniskens P., Lyytinen E., and Baggaley J. (2020). "An outburst of delta Pavonids and the orbit of parent comet C/1907 G1 (Grigg-Mellish)". *Planetary and Space Science*, **189**, article id. 104979.

Jenniskens P. and Vaubaillon J. (2007). "Aurigid predictions for 2007 September 1". *WGN, Journal of the IMO*, **35**, 30–34.

Jenniskens P. and Vaubaillon J. (2008). "Predictions for the Aurigid outburst of 2007 September 1". *Earth, Moon, and Planets*, **102**, 157–167.

Lyytinen E. and Jenniskens P. (2003). "Meteor outbursts from long-period comet dust trails". *Icarus*, **162**, 443–452.

Rendtel J. (1990). "The Alpha Aurigid meteor shower". *WGN, Journal of the IMO*, **18**, 81–84.

Rendtel J. (2007). "Visual observations of the Aurigid peak on 2007 September 1". *WGN, Journal of the IMO*, **35**, 108–112.

Rendtel J. (2020). "2021 Meteor Shower Calendar". International Meteor Organization. IMO_INFO (2-20).

Handling Editor: Javor Kac
This paper has been typeset from a LaTeX file prepared by the authors.

The International Meteor Organization

www.imo.net

Follow us on Facebook InternationalMeteorOrganization

Follow us on Twitter @IMOMeteors

Council

President: Cis Verbeeck,
Bogaertsheide 5, 2560 Kessel, Belgium.
e-mail: cis.verbeeck@scarlet.be

Vice-President: Juraj Tóth,
Fac. Math., Phys. & Inf., Comenius Univ.,
Mlynska dolina, 84248 Bratislava, Slovakia.
e-mail: toth@fmph.uniba.sk

Secretary-General: Robert Lunsford,
14884 Quail Valley Way, El Cajon,
CA 92021-2227, USA. tel. +1 619 755 7791
e-mail: lunro.imo.usa@cox.net

Treasurer: Marc Gyssens, Heerbaan 74,
B-2530 Boechout, Belgium.
e-mail: marc.gyssens@uhasselt.be
BIC: GEBABEBB
IBAN: BE30 0014 7327 5911
Bank transfer costs are always at your expense.

Other Council members:
Javor Kac (see details under WGN)
Detlef Koschny, Zeestraat 46,
NL-2211 XH Noordwijkerhout, Netherlands.
e-mail: detlef.koschny@esa.int
Sirko Molau, Abenstalstraße 13b, D-84072
Seysdorf, Germany. e-mail: sirko@molau.de
Francisco Ocaña Gonzalez, C/ Arquitectura, 7.
28005 Madrid, Spain.
e-mail: francisco.ocana.gonzalez@gmail.com
Vincent Perlerin, 16, rue Georges Bernanos,
51100 Reims, France.
e-mail: vperlerin@gmail.com
Jean-Louis Rault, Société Astronomique de
France, 16, rue de la Vallée, 91360 Epinay sur
Orge, France. e-mail: f6agr@orange.fr
Jürgen Rendtel, Eschenweg 16, D-14476
Marquardt, Germany. e-mail: jrendtel@aip.de

Commission Directors

Visual Commission: Rainer Arlt (rarlt@aip.de)
Generic e-mail address: visual@imo.net
Electronic visual report form:
http://www.imo.net/visual/report/electronic
Video Commission: Sirko Molau (video@imo.net)
Photographic Commission: Bill Ward
(William.Ward@glasgow.ac.uk)
Generic e-mail address: photo@imo.net
Radio Commission: Jean-Louis Rault
(radio@imo.net)
Fireballs: Online fireball reports:
http://fireballs.imo.net

Webmaster

Karl Antier, e-mail: webmaster@imo.net

WGN

Editor-in-chief: Javor Kac
Na Ajdov hrib 24, SI-2310 Slovenska Bistrica,
Slovenia. e-mail: wgn@imo.net;
include METEOR in the e-mail subject line

Editorial board: Ž. Andreić, M. Argo, D.J. Asher,
F. Bettonvil, J. Correira, M. Gyssens,
C. Hergenrother, T. Heywood, J.-L. Rault,
J. Rendtel, C. Verbeeck, S. de Vet, D. Vida.

IMO Sales

Available from the Treasurer or the Electronic Shop on the IMO Website	€	$
IMO membership, including subscription to WGN Vol. 48 (2020)		
Surface mail	26	32
Air Mail (outside Europe only)	49	60
Electronic subscription only	21	25
Proceedings of the International Meteor Conference on paper		
1990, 1991, 1993, 1995, 1996, 1999, 2000, 2002, 2003, per year	9	12
2007, 2010, 2011, per year	15	20
2012, 2013, 2014, 2015 per year	25	34
Proceedings of the Meteor Orbit Determination Workshop 2006	15	20
Radio Meteor School Proceedings 2005	15	20
Handbook for Meteor Observers	15	20
Meteor Shower Workbook	12	16
Electronic media		
Meteor Beliefs Project ZIP archive	6	8

Fireball with comet C/2020 F3 (NEOWISE) from France